Small-strain shear stiffness of compacted bentonites for engineered barrier system

X. Pintado[1], E. Romero[2], J. Suriol[2], A. Lloret[2], B.N. Madhusudhan[3]

[1] AINS Group, Helsinki, Finland, xavier.pintado@ains.fi

[2] Department of Civil and Environmental Engineering, Universitat Politècnica de Catalunya, Barcelona, Spain.

[3] Department of Engineering and the Environment. University of Southampton, Southampton, United Kingdom.

Abstract

The shear modulus (G) of two different bentonites was measured by means of a resonant column apparatus. The samples were compacted at different dry densities and degrees of saturation and tested with different confinement pressures and strains levels for studying the influence of these parameters on the shear modulus. The results show similar tendencies in both bentonites: the shear modulus increases as the dry density increases and exhibits maximum shear modulus when degree of saturation is around 80%. An empirical equation, taking into account the microstructure of the clays, is used to evaluate the shear modulus at small strains as a function of dry density and degree of saturation. Although the values of the shear modulus measured are similar in both bentonites for a given stress and degree of saturation, there is difference in the elastic strain limit of the soil. Bentonite clay is going to be part of the Engineered Barrier System (EBS) in deep geological disposal facilities for the long-term confinement of spent nuclear fuel. In order to fully understand their long-term performance, their behaviour in shearing conditions should be assessed.

Keywords: resonant column; shear modulus; engineered barrier system; suction; effective degree of saturation; macro structure.

Introduction

Deep geological disposal is an option for the long-term confinement of spent nuclear fuel in many countries employing nuclear power. Bentonite is rather complex material that contain a high smectite content and exhibit high plasticity. These materials also contain other clay minerals, e.g., illite, as well as non-clay minerals such as quartz, feldspar, cristobalite, plagioclase and others in small amounts. The complex microstructure and chemical and mineralogical composition of bentonites make it difficult to test and fully interpret their physical behaviour. In particular, the high swelling capacity and low hydraulic conductivity of bentonite materials make difficult to measure mechanical parameters. For this reason, there are a few measures of these parameters available in the literature, in particular, of the shear modulus at small strains.

The minimum density of the bentonite allowed after the saturation process (the bentonite is going to be saturated due to the groundwater flow from the host rock to the bentonite) depends on the requirements for preventing significant microbial activity (it is necessary a minimum swelling pressure for preventing this activity, which depends on the density of the bentonite), ensuring tightness and self-sealing (related to the swelling pressure as well), preventing significant canister sinking (related with the stiffness of the bentonite, which depends on the density) and reducing the colloid-facilitated radionuclide transport and advective transport (the hydraulic conductivity is strongly related to the porosity, which is directly related to the density), but there is also a requirement for the maximum density[1]. The barrier should be soft enough in order to avoid excess of stresses when a fracture intersecting a deposition hole is affected by a nearby earthquake and this fracture slips and causes a shearing of the buffer and the enclosed canister.

48 The current design in Finland and Sweden is nicknamed KBS-3[2]. The KBS-3 design involves
49 the excavation of a tunnels network in a crystalline rock and the emplacement of the canisters
50 containing the spent nuclear fuel in vertical deposition holes (KBS-3V disposal method[3]) or in
51 horizontal galleries (KBS-3H alternative[4]). The canisters containing the spent nuclear fuel are
52 going to be emplaced surrounded by a sealing material called Engineered Barrier System (EBS).
53 This sealing material is compacted bentonite, a high expansive clay. The emplacement of the
54 spent nuclear fuel repository in Finland is planned to be in Olkiluoto[2,4], an island at the western
55 coast. Shear displacements in fractures intersecting a deposition hole and a canister is
56 considered to be one of the canister failure modes. Shear displacements large enough to damage
57 the canister are only possible in large earthquakes. Olkiluoto is located in the Fennoscandian
58 Shield away from active plate margins and is currently seismically quiet. The lack of
59 observations of large post-glacial faults in the Olkiluoto area and in the southern Finland
60 indicates that end-glacial faulting at Olkiluoto seems unlikely, however, the possibility of large
61 earthquakes, especially at the time of ice-sheet retreat, cannot be totally excluded[4]. For KBS-
62 3V, the magnitude of such a rock shear displacement and its rate have been estimated to be at
63 maximum 5 cm and 1.0 m/s, respectively[4].

64 Some studies have been done for the analysis of shearing in canisters. Börgesson[5] presents a
65 mock-up test where the deposition hole was scaled about 1:10 and a copper canister surrounded
66 by expansive clay was sheared under different shear rates. The shearing process was also
67 numerically modelled. Other canister shearing modelling works can be found in Börgesson et
68 al.[6]. The shear modulus is an important parameter and is indirectly introduced with κ_p (related
69 with the volumetric variations with changes in p) and κ_s (related with volumetric variations
70 with changes in suction) if the elastic part of the model is logarithmic elastic for the simulation
71 of bentonite[7]. If the model is linear elastic, the shear modulus can be introduced directly or as

72 function of the Poisson ratio[6]. The shear modulus is related with the Poisson ratio through the
73 equation:

$$G = \frac{E}{2(1+\upsilon)} \qquad (1)$$

74 G depends of the confinement pressure p and the shear strain γ (see equations (7) and (8)).

75 The MX-80 bentonite is one of the bentonites selected as material for the EBS in Finland[2] and
76 in Sweden[1]. This material has high content of smectite (88%), cation exchange capacity (CEC)
77 around 0.86 eq/kg, liquid limit around 500% and plasticity index around 450%. The specific
78 surface is 624 m^2/g. The density of solid particles is 2.78 Mg/m^3. MX-80 can be described as
79 sodium bentonite. More information about the material used in this work can be found in
80 Kiviranta and Kumpulainen[8] and Kiviranta et al.[9].

81 The FEBEX bentonite is the reference material for the EBS in Spain[10]. This material has also
82 high smectite content (92%), cation exchange capacity (CEC) around 1.02 eq/kg, liquid limit
83 around 102% and the plasticity index around 49%. The specific surface is 725 m^2/g. The density
84 of solid particles is 2.70 Mg/m^3. More information about this material can be found in Enresa[10].
85 FEBEX bentonite can be described as calcium bentonite.

86 Triaxial laboratory tests in MX-80 have been carried out for the shearing parameters
87 evaluation[11,12]. The yield parameters are quite well determined by performing triaxial tests but
88 the shear modulus measured can be too low due to the high deformation of the sample when
89 the measures start to be reliable for measuring the shear modulus.

90 Resonant column tests in compacted soils can be found in Edil et al.[13], who used a resonant
91 column device for measuring the shear modulus of samples equilibrated at different suctions in
92 ceramic plate extractors. Wu et al.[14] present resonant column tests in compacted samples tested

93 at controlled water content. More recently, Mancuso et al.[15] and Vassallo et al.[16] developed a
94 suction-controlled resonant column and tested compacted samples.

95 Some resonant column tests have been carried out on MX-80 and FEBEX bentonite samples
96 (Tables 1 and 2). The small-strain shear modulus G_{max} or G_0 of compacted soils depends on dry
97 density, degree of saturation (directly related to the suction through the water retention curve),
98 overconsolidation ratio, confinement pressure, and the way the microstructure (pore size
99 distribution) is organised[17,18], so the tests have been done for different dry densities, degrees of
100 saturation and confinement pressures. The earthquake resistant design also requires the
101 knowledge of the limit strain level, beyond which the material no longer behaves linear elastic[19].

102 Some semi-empirical models have been proposed in order to be able to predict the maximum
103 shear modulus. Many of these models are based on empirical relationships similar to one
104 proposed by Hardin and Black[20]. These empirical expressions are of the following form
105 (Cascante and Santamarina[21]):

$$G_{max} = A\, f(e) p_0^b \qquad (2)$$

106 where p_0 is the isotropic confining load, $f(e)$ is a function of the void ratio and A and b are
107 constant parameters.

108 Recently, some new models have been presented[22] considering the unsaturated state conditions.
109 The results have been usually interpreted in terms of effective stresses or in terms of net stresses
110 and suctions. More recently, Alonso et al.[23] and Heitor et al.[24] proposed the use of a Bishop-
111 type constitutive stress (see equation 9), while Biglari et al.[25,26] used the generalized stress
112 variables proposed by Gallipoli et al.[27].

113 In this work, the effects of the variation of confining pressure, compaction dry density and water
114 content on small strain shear modulus of the two mentioned smectite clays are presented. The

115 results are interpreted using the constitutive stress recently proposed by Alonso et al.[23] and the
116 well-stablished semi-empirical model of Hardin and Black[21].

117 The spent nuclear fuel generates heat and increases the temperature of the buffer and the rock.
118 The maximum temperature is limited to 100ºC and it is expected to be reached 10-20 years after
119 the canister emplacement but this temperature will decrease quite rapidly and in less than 300
120 years, it will be lower than 50ºC and around 35ºC after 1000 years (Ikonen and Raiko[28]). For
121 this reason, the evolution of the shear modulus with the temperature has not been considered.

122 **Experimental methods and results**

123 Stiffness data at different isotropic stresses ranging from p=0.1 to 10 MPa in MX-80 bentonite
124 (tests performed by the Universitat Politècnica de Catalunya with a range of p=0.1 to 0.8 MPa
125 and by the University of Southampton with a range of p=0.4 to 10 MPa) and from p=0.1 to 0.8
126 MPa in FEBEX bentonite (tests performed by the Universitat Politècnica de Catalunya) were
127 determined using a Stokoe-type resonant column under torsional mode of vibration[29]. By
128 varying the frequency of torsional vibration, a frequency response curve at a given torque level
129 can be determined and the resonant frequency associated with the first (fundamental) mode of
130 vibration (f_n) is obtained as the frequency corresponding to the peak response. From the
131 resonant frequency (f_n), the value of shear wave propagation (V_s) within the material and the
132 corresponding shear modulus (G) was calculated using the material geometry with the
133 procedure outlined in ASTM[30]. The damping ratio was also measured but the results and the
134 analysis of the results are out of the scope of this article. Calibration of the resonant column
135 using metal calibration rods and weights of known geometry was performed over the torsional
136 stiffness range exhibited by the bentonite samples[31]. The relation between the shear modulus
137 *(G)* and the resonant frequency *(f_n)* is:

$$G = K f_n^2 \tag{3}$$

where K is a constant which depends of the geometry of the sample and the resonant column test set up (assuming that the polar moment of inertia of the top cap is much greater than that of the soil sample):

$$K = \frac{8\,\pi\,J_m}{R^4} L \tag{4}$$

J_m is the polar moment of inertia of the oscillating top cap, L the length and R the radius of the sample. Circumferential displacement of the top of the sample is measured by an accelerometer.

The average shear strain ($\bar{\gamma}$) is calculated:

$$\bar{\gamma} = \frac{2}{3}\gamma_{max} = \frac{R\,k_{acc}}{12\,\pi^2\,R_a\,L}\frac{V_{pp}}{f^2} \tag{5}$$

f is the frequency of the movement, V_{pp} is the accelerometer output peak to peak voltage, k_{acc} is the calibration constant of the accelerometer output [m s^{-2} V^{-1}] and R_a the distance from the axial axis of the sample to the centroid of the accelerometer.

The MX-80 bentonite was mixed with water till reaching the target water content with a mixer (RV02E Eirich mixer, www.eirich.com). The FEBEX bentonite was mixed with water with a sprayer and a spoon. The material was kept 24 hours covered with a plastic film for avoiding water evaporation after the mixture before sample compaction for improving the mixture of water and soil. The FEBEX powder water content was around 13.0% at laboratory conditions (stored inside plastic bags, the laboratory temperature was around 25ºC and the relative humidity around 50%). Some tests in FEBEX bentonite were performed with a water content lower than 13.0%, in this case, the powder for manufacturing the samples was dried in the oven and the water was added after the powder was cooled. The water content in all cases was also

156 measured following the procedure indicated in ASTM[32]. The samples were uniaxially
157 compacted in steel moulds with pistons in both sides of the sample in order to have as much as
158 uniform dry density distribution and minimize the effect of the friction between mould and soil
159 during the compaction process. All FEBEX and MX-80 samples except samples HP1, HP2 and
160 HP3 had a diameter of 38 mm and height around 78 mm. Samples HP1, HP2 and HP3 had a
161 diameter of 50 mm and height around 100 mm (they were tested in another resonant column
162 with higher confinement pressure capacity).

163 The Proctor plane was used to map different initial states, which covered a dry density range
164 between 1.43 and 1.75 Mg/m^3 with degrees of saturation between S_r=51% and 96% in MX-80
165 bentonite (Figure 1) and a dry density range between 1.54 and 1.74 Mg/m^3 with degrees of
166 saturation between S_r=11% and 86% in FEBEX bentonite. The exact target dry density in
167 compacted soils is difficult to reach due to the rebound effect: the samples expand when are
168 extracted after the compaction process. This expansion cannot be controlled and for this reason
169 it is not possible to have a set of samples with exactly the same dry density. This density was
170 calculated with the dimensions of the samples after the compaction.

171 For a given water content and dry density, the pore distribution is not the same in the samples
172 compacted for the resonant column tests as would be expected for the buffer blocks. This
173 difference may result in different pore distributions because the initial water content and the
174 history of the water content changes are different. This could also have influenced the water
175 retention curve measurement because the initial state of the bentonite in the deposition holes is
176 different than the initial state of the samples when the water retention curve was measured,
177 which was drier. This is due to the hysteresis of the water retention curve: when the sample
178 starts wetting, it does not follow the main wetting path from the beginning, it starts moving
179 from a point between the main drying path and main wetting path till reaching the main wetting
180 path. When the water retention curve is measured drying or wetting the sample from a certain

181 degree of saturation, the final state could be on the hysteresis path, without reaching the main
182 drying or wetting path (Seiphoori et al.[33]). More information about the water retention curve in
183 MX-80 and FEBEX can be found in Kiviranta et al.[9] and Enresa[10] respectively.

184 The confining (isotropic) pressure on the soil was applied using compressed air. The valves for
185 drainage were open till reaching the steady state conditions in vertical displacements and
186 remained open during the measurement of the shear modulus. The water content was considered
187 constant (no drainage was expected because the samples were in unsaturated conditions). For
188 measuring the changes in height of the sample during the consolidation stages, a displacement
189 sensor (LVDT) was incorporated in the setups for MX-80 samples. The time evolution of the
190 vertical strain was measured in all the samples in order to control the time needed to reach the
191 end of the consolidation period after the isotropic stress increments and to assure that the water
192 pressure reached the steady state conditions.

193 The time required for the consolidation of the samples was variable due to differences in the
194 degree of saturation and dry density of the samples. Figure 2 shows the time required to perform
195 each MX-80 test with different pore pressure equalisation stages (four confining stresses at the
196 Universitat Politècnica de Catalunya and five at the University of Southampton) as a function
197 of the degree of saturation. As confinement pressure was applied using dry compressed air, in
198 the long duration tests some small mass of water was lost due to vapour diffusion (evaporation)
199 through the latex membrane. The tests done in high pressure cell had a membrane of butyl to
200 minimize the water mass loss. The maximum water mass loss was 2.5% after 23 days of
201 consolidation.

202 The vertical strains (ε_z) as function of the confinement pressures are presented in Figure 3.
203 Some selected MX-80 samples have been represented (no measures were taken with FEBEX
204 bentonite). This dependence can be approximated by the function:

$$\varepsilon_z = \alpha + \beta \ln(p) \quad (6)$$

The relation $\beta = \Delta\varepsilon_z / \Delta ln(p)$ is plotted in Figure 4. Values from 1.5×10^{-3} to 0.8×10^{-3} have been obtained for the parameter β in the range of dry densities from 1.55 to 1.7 Mg/m^3 and for degrees of saturation between 51 and 96%. The tests done with high pressure test set-up are not at the same tendency due to the value of the slope β is higher for the highest confinement pressures showing an "apparent preconsolidation pressure" that ranges between 400 to 1000 kPa depending on dry density and water content of the samples. This behaviour was not expected due to the high compaction pressures applied when the samples were prepared, especially in high density. The axial compaction pressure was expected to be higher than 10 MPa[34].

The value of $\kappa = \Delta e / \Delta ln(p)$ was calculated[35] in isotropic tests on MX-80. For comparing β (equation 4) with κ, the following relation should be used:

$$\kappa = \frac{3\beta}{\rho_d / \rho_s} \quad (5)$$

where ρ_d and ρ_s are the dry and solid densities, respectively. The material is considered isotropic, that is, the strains are the same in the three principal axes when the stress applied on the sample is isotropic.

The average value of κ calculated[35] for a degree of saturation of 51% and dry density of 1.82 Mg/m^3 was $\kappa = 7.5\times10^{-3}$ ($\beta = 1.7\times10^{-3}$). This value is close to values presented in Figure 4 but higher in many cases. Although the dry density is slightly higher[35], its degree of saturation is lower and it could have the effect of reducing the stiffness of the sample. The values of κ calculated in high pressure tests are higher because they could include also the effect of visco-plastic strains.

The confinement pressure reduces the porosity and increases the dry density. The degree of saturation also increases due to the water content remains constant in all test. It is possible to calculate the volumetric strain assuming a value for the bulk modulus in the confinement pressure step. If the material is considered as isotropic and linear elastic, the bulk modulus (K) can be calculated with the equation:

$$K = \frac{p}{3\epsilon_z} \tag{6}$$

The material was compacted uniaxially, so the hypothesis of isotropic behaviour could not be true. There are a few tests which study the anisotropy of the bentonite due to the compaction process. In FEBEX bentonite, Villar[36] measured the hydraulic conductivity and swelling pressure among other properties in samples drilled in blocks compacted uniaxially. The samples were drilled parallel and perpendicular to the compaction direction. The results showed that there does not seem to be significant anisotropy in FEBEX samples. In MX-80 bentonite, some measures of uniaxial compression tests were done in samples compacted by different ways[37]. The results did not show anisotropy in MX-80 samples and, with the hypothesis of isotropy, the bulk modulus was calculated.

The shear modulus at small strain (~10^{-4} %), G_0, as function of the confinement pressure is plotted in Figure 5 and Figure 6 for MX-80 and FEBEX bentonites, respectively. The shear modulus increases with the confinement pressure as expected. The results are presented in Tables 1 and 2 as well.

The small-strain shear modulus as function of the degree of saturation is shown in Figure 7 when the confinement pressure is 800 kPa. In this Figure, the changes in the degree of saturation due to compressibility of MX-80 are considered, for FEBEX bentonite the initial degrees of saturation have been plotted. The changes in volume during the tests are small and it can be

247 seen that they do not alter the tendency of the results. On the other hand, from the figures it is
248 clear than the shear modulus increases with the dry density.

249 The small-strain shear modulus for a confinement stress of 800 kPa is also plotted in a
250 compaction plane and in a contour plot (Figure 8) as function of dry density and degree of
251 saturation. The MX-80 small-strain shear modulus seems to have a maximum for degrees of
252 saturation around 75%. The contour plots in FEBEX bentonite do not give a clear tendency
253 with regards to the degree of saturation. For both clays, the stiffness increases when the dry
254 density increases.

255 This behaviour is not consistent with the results presented by Suriol et al.[17] and Hoyos et al.[18],
256 who show a monotonic increase of the shear modulus with the increase of the suction, which is
257 equivalent to a decrease of the degree of saturation. Merchán[38] measured the shear modulus for
258 moderately swelling clay (Boom clay, Romero et al.[39]) and a maximum in shear modulus as
259 function of the degree of saturation was measured. It should be taken into account that the soil
260 tested by Suriol et al.[17] was low plasticity silty clay (CL following the USCS) and the soil tested
261 by Hoyos et al.[18] was silty sand (SM following the USCS) while the Boom clay has a plasticity
262 closer to the FEBEX bentonite.

263 **Interpretation of the results**

264 The relationship between the confinement pressure p expressed in MPa and the small-strain
265 shear modulus G_0 can be related by power law function (see equation (2)):

$$G_0 = G_{0.1}(p/0.1)^n \qquad (7)$$

266 where the parameter $G_{0.1}$ is associated with the value of the initial shear modulus at the reference
267 confinement pressure of 0.1 MPa and n is a parameter which takes into account the increase of
268 the shear modulus with the confinement pressure. Figure 9 shows that the parameter n seems

to decrease when the degree of saturation increases in FEBEX bentonite (about 0.6 for S_r =60% and 0.1 to 0.2 for S_r greater than 80%) but any clear tendency cannot be seen for MX-80.

The variation of the shear modulus (G) with the shear strain (γ) is shown in Figure 10 for a confinement stress of 800 kPa. The shear modulus begins to reduce when the shear strain increases beyond certain strain level, below which the material exhibits linear elastic behaviour. Going through the Figure 11, it is possible to see that this threshold strain ranges between 10^{-3} % and 20×10^{-3} % for MX-80 and from 10^{-3} % to 200×10^{-3} % in the case of FEBEX bentonite. This difference could be attributed to the soil plasticity, indicated by plasticity index of the soil. Plastic Index of MX-80 is 450% against 49% for FEBEX bentonite, indicating 10-fold difference in the index value and thus the shift in their threshold shear strain level. Vucetic and Dobry[39] showed higher values of G/G_0 for the same value of shear strain when the plasticity index is higher although this result was in contradiction with the results from Kagawa[40], probably due to the scatter of the results.

In Figure 11, the ratio G/G_0 is compared with other studies as well. The soils are quite different but it is possible to see that the results are between the extreme values presented by Suriol et al.[17] in a CL material with a confinement pressure of 200 kPa, Borden et al.[42] for a piedmont residual soil (MH, with a confinement pressure of 100 kPa) and Kagawa[40] for a marine clay (MH with a consolidation stress between 50 and 1400 kPa) showed values close to the values presented by the MX-80 and FEBEX bentonites. It is also important to consider that the maximum shear modulus (G_0) measured in bentonites is higher than the G_0 measured in soils tested by these authors, so Borden et al.[42] measured a G_0 around 45 MPa, Suriol[17] around 50 MPa and Kagawa[40] presented a wide range of results, up to 120 MPa. The ratio G/G_0 presented in Figure 11 can also be compared with the results presented in Vucetic and Dobry[39], however, the results reported by these authors do not pertain to bentonite clays, which have usually higher plasticity index than the maximum reported in their work (around 100%). Only the 0.01% shear

strain can be compared as it was not possible to reach 0.1% shear strain in the resonant column tests performed in this work. The range of G/G_0 measured in MX-80 was between 0.77-0.98 but with the average closer to 0.98 than to 0.77 and in FEBEX bentonite it was between 0.75-0.93 with the average closer to 0.93 than to 0.73. The ranges expected from Vucetic and Dobry[39] are between 0.95-1 for MX-80 (plasticity index higher than 150%) and 0.85-1 for FEBEX bentonite (plasticity index around 50%). Although the scatter of the measurements is high, it is possible to conclude that the results are close to the values expected from Vucetic and Dobry[39] and the lower values of G/G_0 correspond to the bentonite with lower plasticity index. It should also be said that other bentonites have been reported to have high plasticity indices, especially sodium bentonites. For example, sodium GMZ bentonite has a plasticity index of 239% and calcium GMZ bentonite only 58%, Sun et al.[41]. Another example is Akagi calcium bentonite with a plasticity index of 268% and Kunigel sodium bentonite at 471%, Shirazi et al.[42].

To analyse the variation of the shear modulus with the strain level, the "hardening soil model with small strain stiffness" used in PLAXIS[43] can be used:

$$G(\gamma) = \frac{G_0}{1 + 0.385\frac{\gamma}{\gamma_{0.7}}} \qquad (8)$$

where $\gamma_{0.7}$ corresponds to the strain at which the modulus G is $0.722G_0$. This equation is similar to the equation presented by Borden et al.[44] but with two parameters less. The Figure 12 presents the test results and predicted values using this model for some tests and Figure 13 shows a correlation between the parameter $\gamma_{0.7}$ and the shear modulus at small strains. $\gamma_{0.7}$ varies between 0.01% in samples with a maximum shear modulus of about 200 MPa to 0.1% in samples with a maximum shear modulus about 400 MPa.

The value of $\gamma_{0.7}$ can be assessed. The values measured at high-range of strains are closer to the values calculated from these authors than the values measured at low-range. The relation between the plastic index and $\gamma_{0.7}$ as a parameter that indicates how the shear modulus drops when the shear strains increase is presented in Figure 14. The tests presented by Kagawa[40] were performed in saturated conditions, with a wide range of dry densities (1.1-1.6 Mg/m^3) and a plastic index between 23 and 36%. The tests presented by Borden et al.[44] were performed in unsaturated conditions (degree of saturation between 66-88%) and a dry density between 1.02 and 1.2 Mg/m^3. The results presented by Suriol et al.[17] correspond to a material with a degree of saturation of 80%, dry density between 1.65 and 1.85 Mg/m^3 and plastic index of 12%. Despite the dispersion due to the effects of dry density and saturation of the different samples, a tendency of increase of $\gamma_{0.7}$ with soil plasticity is clear, according with the results of Vucetic and Dobry[39].

To interpret the effects of the degree of saturation and confinement stress, the model presented by Alonso et al.[22] has been selected. These authors suggested that unsaturated soil behaviour may be modelled in terms of two independent fields. 1) Constitutive stress ($\overline{p}$):

$$\overline{p} = p - P_g + \overline{S_r} s \qquad (9)$$

and 2) effective suction ($\overline{s}$):

$$\overline{s} = \overline{S_r} s \qquad (10)$$

where p is the total mean stress, P_g is the gas pressure (0 for atmospheric conditions) and s the suction.

The effective degree of saturation $\overline{S_r}$ was introduced by Romero and Vaunat[45] and indicates the "degree of saturation" of the macroscopic level in a double structured soil. In the framework of the model of Alonso et al.[22], only the water which fills the macropores has mechanical effects.

335 At low degrees of saturation, the water fills the micropores in the clay aggregates, but the water
336 content of the aggregates has no influence on the global mechanical behaviour[23]. This approach
337 may be appropriate when the soil has a clear double structure, such as compacted bentonites.

338 According to Alonso et al.[22], the effective degree of saturation can be expressed by the
339 following equation:

$$\overline{S_r} = \frac{S_r - \xi_m}{1 - \xi_m} + \frac{1}{n_s} ln\left[1 + exp\left(-n_s \frac{S_r - \xi_m}{1 - \xi_m}\right)\right] \quad (11)$$

340 where $\xi_m = e_m/e$ is a microstructural state variable that indicates the ratio between the
341 microstructural void ratio (e_m) and the total void ratio (e). n_s is a model parameter that defines
342 the degree of smoothing of Equation (11) around point $S_r=\xi_m$. The value chosen for n_s is 3 as
343 in Alonso et al.[22].

344 The e_m can be calculated from the pore size distribution obtained by the mercury intrusion
345 porosimety (MIP). As a first approximation, a linear relationship between e_m and e_w (water
346 volume / solid volume ratio defined as $V_w/V_s = e\,Sr$) can be proposed[46]:

$$e_m = e_m^* + \beta_m \langle e_w - e_m^* \rangle \quad (12)$$

347 where $\langle\,\rangle$ designates the Macauly brackets (ramp function). For $e_w<e_m^*$ a constant $e_m=e_m^*$
348 results. According to Figure 15, for a dry sample compacted in MX-80 with a dry density of
349 1.80 Mg/m^3, the e_m is 0.29 (as compacted). Fixing this value as e_m^*, β_m can be calculated and
350 its value is 0.55. The values of e_m^* and β_m are 0.53 and 0.40 in FEBEX bentonite[47]. The analysis
351 of Figure 16 gives similar values. The e_m can also be calculated from the water retention
352 curve[48,49] (and Figure 15 and Figure 16). In this approach, the microporosity is evaluated taking

into account the water content for which the effect of dry density (macroporosity) has not effect in water retention curve.

According to the empirical proposal[20] and using the constitutive stress ($\overline{p}$)[22], shear modulus at very small strains (G_0), can be obtained using the following empirical equation:

$$G_0 = C\frac{(A - e_M)^B}{1 + e_M}\left(\frac{\overline{p}}{p_{ref}}\right)^{1/2} OCR^k p_{ref} \qquad (13)$$

where A, B and C are constants depending of the soil, e_M the macrostructural void ratio (e-e_m), parameter k depends on clay plasticity index. For a plasticity index of higher than 100 (MX-80), the value of k is 0.5 and for a plasticity index between 40 and 60 (FEBEX), the value is 0.355[20]. p_{ref} is a pressure reference (usually 100 kPa) and the overconsolidation ratio (OCR) is defined as $\overline{p_{max}}/\overline{p}$. In the case of compacted sample, $\overline{p_{max}} = p_{compaction} + s\overline{S_r}$. The compaction pressure in MX-80 bentonite has been evaluated[37] and the compaction pressure in FEBEX bentonite has also been evaluated[50]. The more compaction pressure is the more G_0 obtained. The sample suctions have been calculated from the water retention curve of each bentonite and the changes in dry density due to the increase in confinement stress have been discarded.

The selected values of the constants *A, B* and *C* are the same presented Vucetic and Dobry[39] for overconsolidated clays. The values of the parameter k have been obtained using a least square procedure with the measured values of G_0. The obtained values of the parameters are shown in Table 3. Finally, the values of G_0 measured and calculated are also presented in the compaction plane shown in Figure 17. The calculated isolines show a tendency of shear modulus increment when the water content or the dry density increases.

Figure 18 illustrates the contribution of constitutive confining stress, overconsolidation ratio and macrovoid ratio to rigidity changes. For a given dry density, the major influence on shear

modulus is due to constitutive confining stress. In FEBEX clay a clear maximum for a degree of saturation of 80% can be observed. For high degrees of saturation, the decrease of suction prevails whereas for low degrees of saturation, the effective saturation degree tends to be small. In the MX-80 clay, only the effects of the suction decrement when the degree of saturation is high can be appreciated. The effect of overconsolidation ratio has a minimum for a degree of saturation near 80% where the compaction effort was minimum, in a similar process than the one observed in the optimum of Proctor curves. For a constant dry density, the effect of macrovoid ratio is only appreciable for high degrees of saturation, where e_w is higher than e_m*.

Conclusions

The measurement of the small-strain shear modulus has been done for two different bentonites which are candidates for the Engineered Barrier System in a deep geological spent nuclear fuel disposal, the MX-80 in Sweden and Finland and the FEBEX in Spain. The shear moduli measured are relatively high for a plastic clay, probably due to the high dry densities reached (the compaction degree is quite high) and the high ranges of suctions in bentonites[22,48]. The shear modulus increases with the dry density and the confinement pressure as it was expected but the experimental results do not show a clear tendency with the degree of saturation. In the case of MX-80 bentonite, for a given dry density a maximum value of rigidity may be observed when the degree of saturation is around 70-80% whereas in the case of FEBEX bentonite this maximum is less evident. Some authors indicate that the shear modulus increases with the suction (or when the degree of saturation reduces) but other authors indicate that the shear modulus has a maximum with relative low degrees of saturation, probably due to the different type of soils presented in different works. The tests presented in this work do not cover the full range of suctions.

The relation between the plastic index and $\gamma_{0.7}$, which indicates how the shear modulus drops with the shear strains is not clear. Most of the values of $\gamma_{0.7}$ measured in FEBEX bentonite were lower than the values measured by Kagawa (1992) although its plasticity index is higher. The values of $\gamma_{0.7}$ measured in MX-80 varied over a wide range. The value of the plasticity index for bentonites is high, so it is possible that a correlation between this parameter and $\gamma_{0.7}$ cannot be reasonably stablished.

Although the scatter in the measures is significant, it is possible to assign a limiting value for the shear modulus and predict the evolution as a function of the shear strains and the confinement pressure from equations (7) and (8) in order to have a safety value for the stresses developed in the canister containing the spent nuclear fuel during an earthquake.

The proposed model can be a useful tool to interpret the test results and allows the researchers interested in the measurement of the shear modulus to evaluate the effects of relevant variables (water content, dry density, compaction effort and confining stress) on this parameter.

Acknowledgements

Financial support of POSIVA Oy (Finland) through a collaboration agreement with B+TECH Oy (now Saanio & Riekkola Oy) and CIMNE (Spain) “Small-strain stiffness of statically compacted MX-80 bentonite using resonant column tests” (2013-2014) and a second collaboration agreement with the University of Southampton (United Kingdom) “Shear modulus and damping properties of unsaturated bentonite” are greatly acknowledged. Authors appreciate the management work from Kari Koskinen (POSIVA, Oy).

References

[1] Posiva. Safety Case for the Disposal of Spent Nuclear Fuel at Olkiluoto. Performance Assessment 2012. Posiva Report 2012-04. Eurajoki, Finland; 2012.

[2] SKB. Design, production and initial state of the closure. SKB Technical report TR-10-17, Stockholm, Sweden; 2010.

[3] Juvankoski M, Marcos N. Design Basis for Buffer Components. Posiva Working report 2009-132, Eurajoki, Finland; 2010.

[4] Posiva. KBS-3H Complementary Studies 2008-2010. Posiva Report 2013-03, Eurajoki, Finland; 2013.

[5] Börgesson L. Model Shear Tests of Canisters with Smectite Clay Envelopes in Deposition Holes. SKB Technical Report 86-26, Stockholm, Sweden; 1986.

[6] Börgesson L, Johannesson LE, Hernelind J. Earthquake induced rock shear through a deposition hole. Effect on the canister and the buffer. SKB Technical report TR-04-02, Stockholm, Sweden; 2004.

[7] Alonso, E., Gens, A., Josa, A. A constitutive model for partially saturated soils. *Géotechnique* 1990; 40(3): 405-430

[8] Kiviranta L, Kumpulainen S. Quality Control and Characterization of Bentonite Materials. Posiva Working report 2011-84, Eurajoki, Finland; 2011. Material codes Be-Wy—VT0002-BT1, BT2 and BT3-Sa-R.

[9] Kiviranta L, Kumpulainen S, Pintado X, Karttunen P, Schatz T. Characterization of bentonite and clay materials 2012 - 2015. Posiva working report 2016-05, Eurajoki, Finland; 2016.

[10] Enresa. FEBEX project. Full-scale engineered barriers experimental for a deep geological repository for high level radioactive waste in crystalline rock. Final Report. Enresa technical publication 1/2000; Madrid, Spain; 2000.

442 [11] Börgesson L, Johanesson LE, Sandén T, Hernelind J. Modelling of the physical behaviour
443 of water saturated clay barriers. Laboratory tests, material models and finite element
444 application. SKB Technical report TR-95-20, Stockholm, Sweden; 1995.

445 [12] Dueck A, Börgesson L, Johannesson LE. Stress-strain relation of bentonite at undrained
446 shear. Laboratory tests to investigate the influence of material composition and test
447 technique. SKB Technical report TR-10-32, Stockholm, Sweden; 2010.

448 [13] Edil TB, Motan SE, Toha FX. Mechanical behaviour and testing methods of unsaturated
449 soils. *In R.N. Yong & F.C. Townsend (eds), Laboratory of strength of soil ASTM STP*
450 1981;740:114-129. Philadelphia: American Society for Testing and Materials.

451 [14] Wu S, Gray DH, Richart FE. Capillary effects on dynamic modulus of sands and silts.
452 *Journal of Geotechnical engineering division ASCE* 1984;119(9):1188-1203.

453 [15] Mancuso C, Vassallo R, d'Onofrio A. Small strain behaviour of a silty sand in controlled-
454 suction resonant column-torsional shear tests. *Canadian Geotechnical Journal*
455 2002;49(2):226-243.

456 [16] Vassallo R. Mancuso C. Vinale F. Effects of net stress and suction history on the small
457 strain stiffness of a compacted clayey silt. *Canadian Geotechnical Journal*
458 2007;44(4):447-462.

459 [17] Suriol J, Romero E, Lloret A, Vaunat J. Small-strain shear stiffness of compacted clays:
460 Initial state and microstructural features. *Proceedings of the 6th International Conference*
461 *on Unsaturated Soils, Sydney, 2014. Unsaturated Soils: Research and Applications, Taylor*
462 *& Francis Group, London* 2014;(1):769-775.

463 [18] Hoyos RL, Suescún-Florez EA, Puppala AJ. Stiffness of intermediate unsaturated soil from
464 simultaneous suction – controlled resonant column and bender element testing.
465 *Engineering Geology* 2015;188:10-28.

466 [19] Madhusudhan BN, Kumar J. Damping of Sands for Varying Saturation. *Journal of*
467 *Geotechnical and Geoenvironmental Engineering* 2013;139(9):1625-1630.

468 [20] Hardin BO, Black WL. Closure to vibration modulus of normally consolidated clay.
469 *Journal of Geotechnical Engineering ASCE* 1969;95(6):1531-1537.

470 [21] Cascante G, Santamarina JC. Interparticle contact behaviour and wave propagation.
471 *Journal of geotechnical engineering* 1996;122(10):831-839.

472 [22] Alonso EE, Pinyol NM, Gens, A. Compacted soil behaviour: initial state, structure and
473 constitutive modelling. *Géotechnique* 2013;63(6):463–478.

474 [23] Alonso EE, Pereira JM, Vaunat J, Olivella S. A microstructrally based effective stress for
475 unsaturated soils. *Géotechnique* 2010;60(12):913-925.

476 [24] Heitor A, Indraranta B, Cholacht C. Laboratory study of small-strain behaviour of a
477 compacted silty sand. *Canadian Geotechnical Journal* 2013;50:179-188.

478 [25] Biglari M, Ashayeri I. An empirical model for shear modulus and damping ratio in
479 unsaturated soils. *In Jotisankasa, Sawangsuriya, Soralump and Mairaing (eds).*
480 *Unsaturated Soils: Theroy and Practice*, 2011;591-595. Kesetsart University, Thailand.

481 [26] Biglari M, Mancuso C. d'Onofrio A, Javari MK, Shafiee A. Modelling the initial shear
482 stiffness of unsaturated soils as a function of the coupled effects of the void ratio and the
483 degree of saturation. *Computers and Geotechnics* 2011;38(5):709-720.

[27] Gallipoli D, Gens A, Sharma R, Vaunat J. An elastoplastic model for unsaturated soils incorporating the effect of suction and degree of saturation on mechanical behaviour. *Géotechnique* 2003;53(1):123-155.

[28] Ikonen, K., Raiko, H. Thermal dimensionin of Olkiluoto repository for spent fuel. Posiva working report 2012-56. Eurajoki, Finland; 2012.

[29] Anderson DG, Stokoe KH, 1978. Shear modulus: A time-dependent soil property. *ASTM Special Technical Publication 'Dynamic Geotechnical Testing'* 1978;654:66-90.

[30] ASTM. Standard test methods for modulus and damping of soils by the resonant-column method. Annual book of ASTM STANDARDS, Vol. 04·08, D-4015. Philadelphia: American Society for Testing and Materials; 2001.

[31] Clayton CRI. Stiffness at small strain: research and practice. *Géotechnique* 2011;61(1):5-37.

[32] ASTM. Standard test methods for laboratory determination of water (moisture) content of soil and rock by mass. ASTM D2216-10 standard. Philadelphia: American Society for Testing and Materials; 2010.

[33] Seiphoori, A., Ferrari, A., Laloui, L. Water retention behaviour and microstructural evolution of MX-80 bentonite during wetting and drying cycles. *Géotechnique* 2014;64(9): 721-734.

[34] Johanesson LE, Börgesson L, Sandén T. Compaction of bentonite blocks. Development of technique for industrial production of blocks which are manageable by man. SKB Technical report TR 95-19, Stockholm, Sweden; 1995.

505 [35] Tang AM. *Effect de la temperature sur le comportement des barrières de confinement*.
506 [Ph.D thesis]. Paris, France: École Nationale des Ponts et Chaussées; 2005.

507 [36] Villar MV. Thermo-hydro-mechanical characterisation of a bentonite from Cabo de Gata.
508 A study applied to the use of bentonite as sealing material in high level radioactive waste
509 repositories. Publicación Técnica ENRESA 01/2002. 258 pp. Madrid. Spain; 2002.

510 [37] Johanesson LE. Compaction of full size blocks of bentonite for the KBS-3 concept. Initial
511 tests for evaluation technique. SKB Report R 99-66, Stockholm, Sweden; 1999.

512 [38] Merchán V. *Small strain stiffness and residual strength of unsaturated Boom clay: a micro-*
513 *structural insight*. [Ph.D thesis]. Barcelona, Spain: Technical University of Catalonia;
514 2011.

515 [39] Romero E, Gens A, Lloret A. Water permeability, water retention and microstructure of
516 unsaturated compacted Boom clay. *Engineering Geology* 1999; 54:117-127.

517 [40] Kagawa T. Moduli and damping factors of soft marine clays. *Journal of Geotechnical*
518 *Engineering* 1992;118(9):1360-1375.

519 [41] Sun, De'an, Sun, W, Fang, L. Swelling characteristics of Gaomiaozi bentonite and its
520 prediction. Journal of Rock Mechanics and Geotechnical Engineering 2014; 6:113-118.

521 [42] Shirazi, SM, Kazama, H, Salman, FA, Othman, F, Shatirah, A. Permeability and swelling
522 characteristics of bentonite. International Journal of the Physical Sciences
523 2010;5(11):1647-1659.

524 [43] PLAXIS, 2015. Material models manual. http://www.plaxis.nl/files/files/2D-3-Material-
525 Models.pdf

526 [44] Borden, RH, Shao, L., Gupta, A. Dynamic properties of piedemont residual soils. Journal
527 of Geotechnical Engineering 1996; 122(10): 813-821.

528 [45] Romero E, Vaunat J. Retention curves in deformable clays. In A. Tarantino and C.
529 Mancuso (eds). Experimental evidence and theoretical approaches in unsaturated soils
530 2001; 91-106. Rotterdam. A.A. Balkema.

531 [46] Romero E, Della Vecchia G, Jommi C. An insight into the water retention properties of
532 compacted clayey soils. *Géotechnique* 2011;61(4):313-328.

533 [47] Romero E. A microstructural insight into compacted clayey soils and their hydraulic
534 properties. *Engineering Geology* 2013;165:3-19.

535 [48] Navarro V, Asensio L, De la Morena G, Pintado X, Yustres A. Differentiated intra- and
536 inter-aggregate water content models of MX-80 bentonite. *Applied Clay Science*
537 2015;118:325-336.

538 [49] Lloret A, Villar MV, Sanchez M, Gens A, Pintado X, Alonso EE. Mechanical behaviour
539 of heavily compacted bentonite under high suction changes. *Géotechnique* 2003;53(1):27–
540 40.

541 [50] Villar MV, Lloret A. Influence of dry density and water content on the swelling of a
542 compacted bentonite. *Applied Clay Science* 2008;39:38–49.

543 [51] Pintado, X., Kristensson, O., Malmberg, D., Åkesson, M., Olivella, S., Puig, I. TH and
544 THM modelling of a KBS-3H deposition drift. Posiva working report 2016-25, Eurajoki,
545 Finland; 2018.

546

547

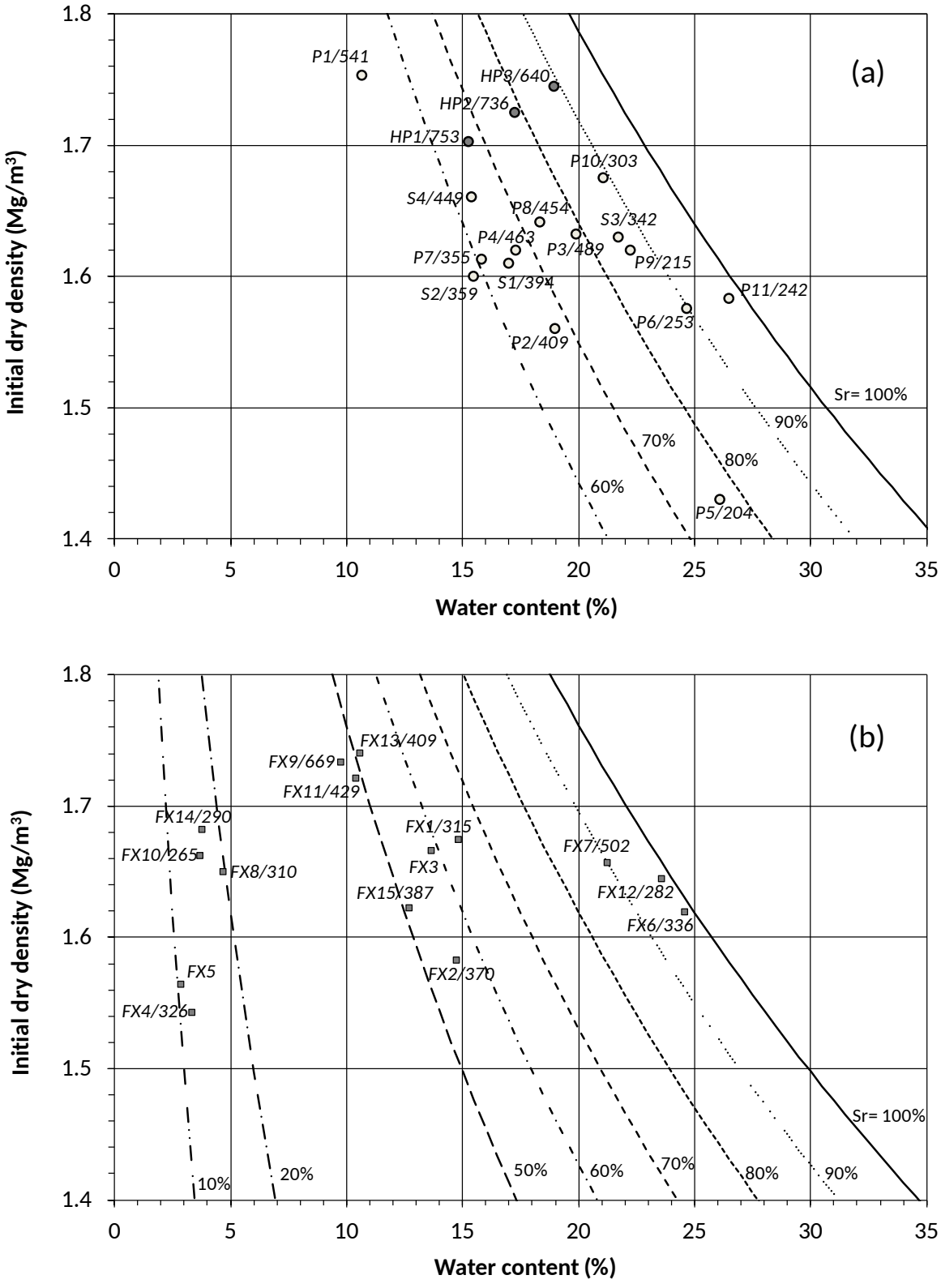

548 Figure 1. Water contents and dry densities of MX-80 (a) and FEBEX (b) tested samples shown in a
549 compaction plot. The number with the reference of the sample is G_0 (MPa) when the confinement
550 pressure was 800 kPa.

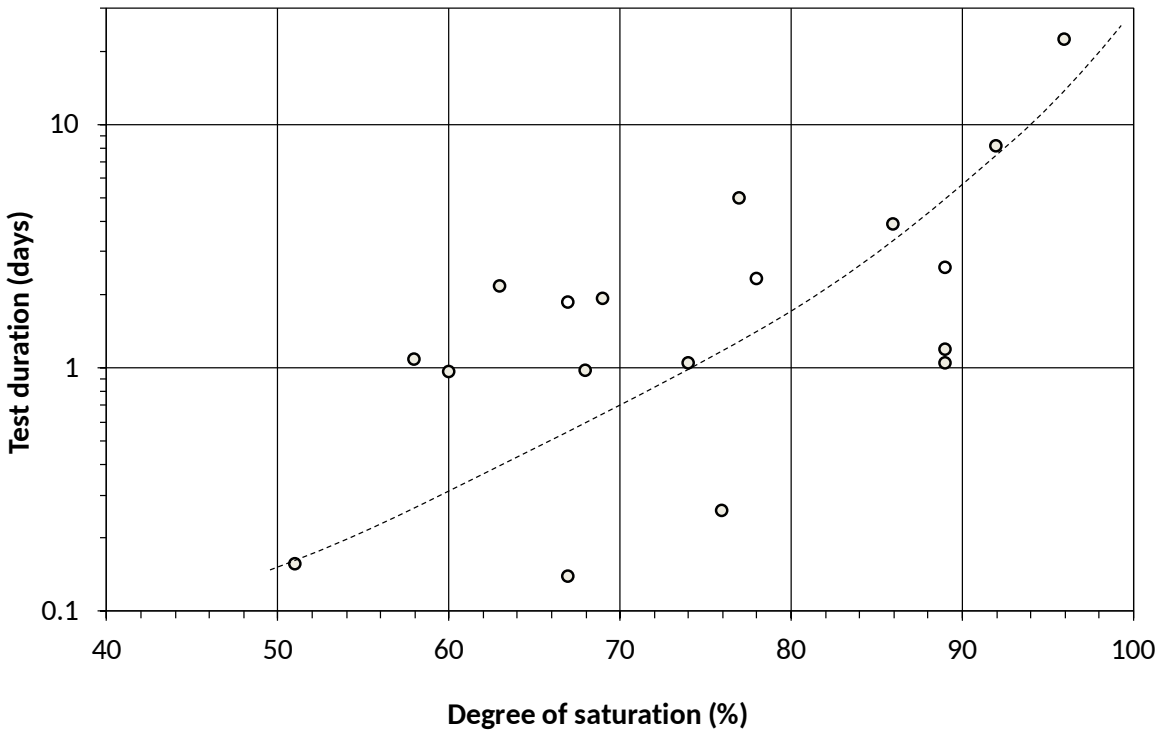

551

552 Figure 2. Time required for performing the tests in order to reach the steady state conditions when there
553 was consolidation due to the sample loading.

554

555

556

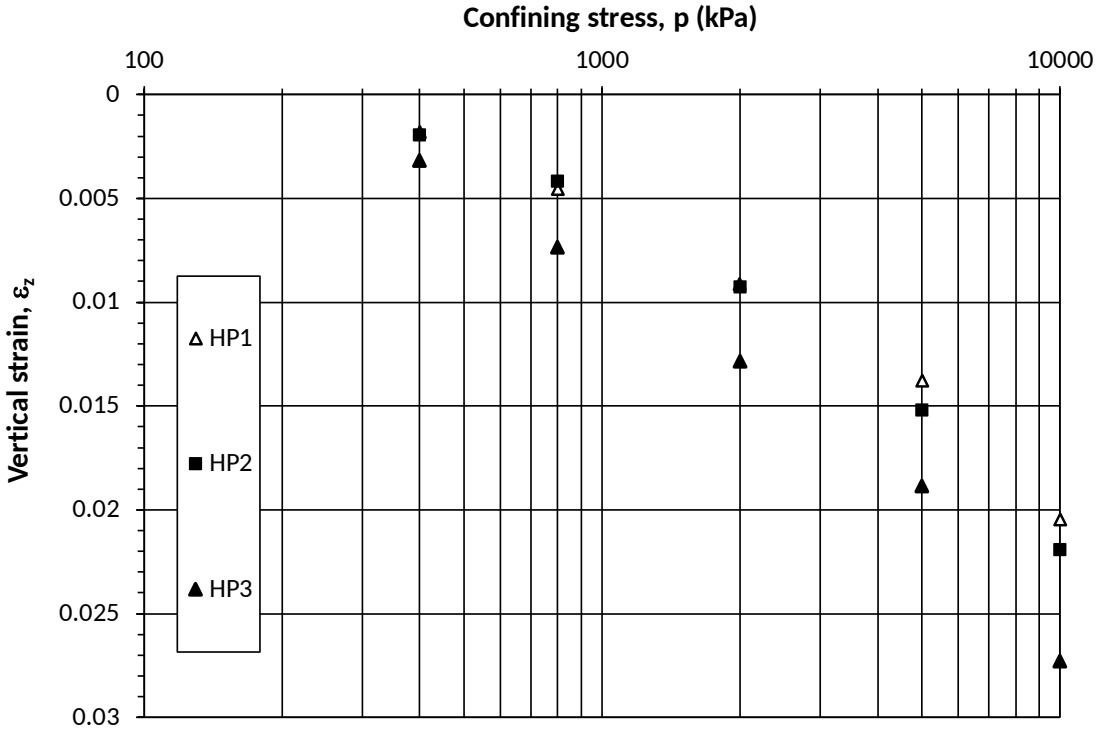

557

558 Figure 3. Relationship between isotropic mean stress (p) and vertical strain (ε_z) for selected MX-80
559 samples.

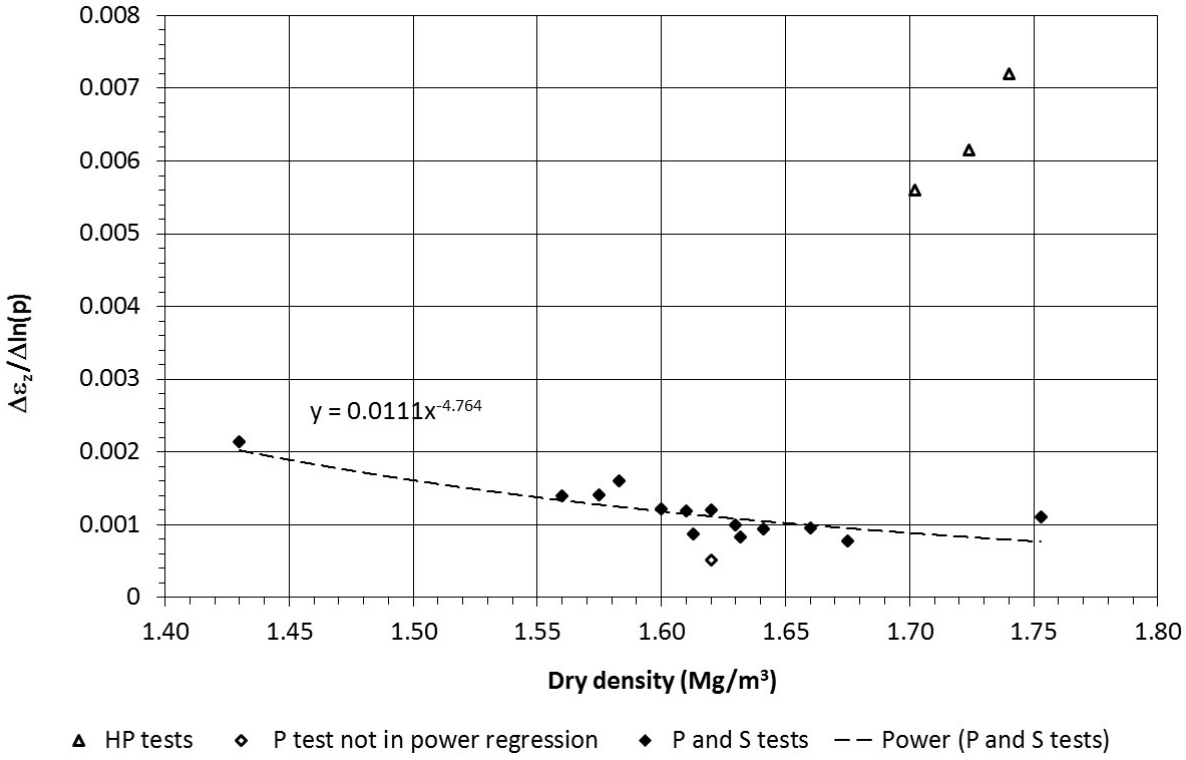

560

561 Figure 4. Relationship between isotropic mean stress (p) and vertical strain (ε_z) for selected MX-80
562 samples. HP tests were made in high-pressure test set-up and the tests P and S were done with the low-
563 pressure test set-up (P first series and S second series).

564

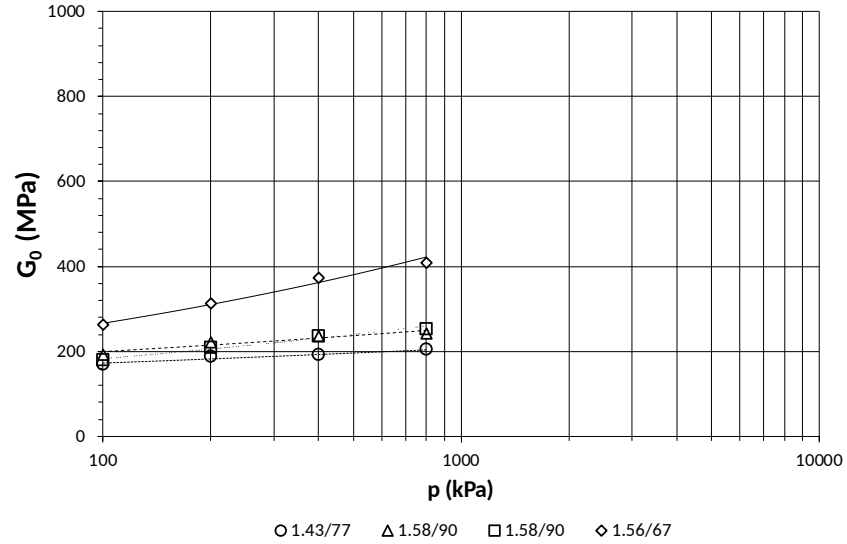

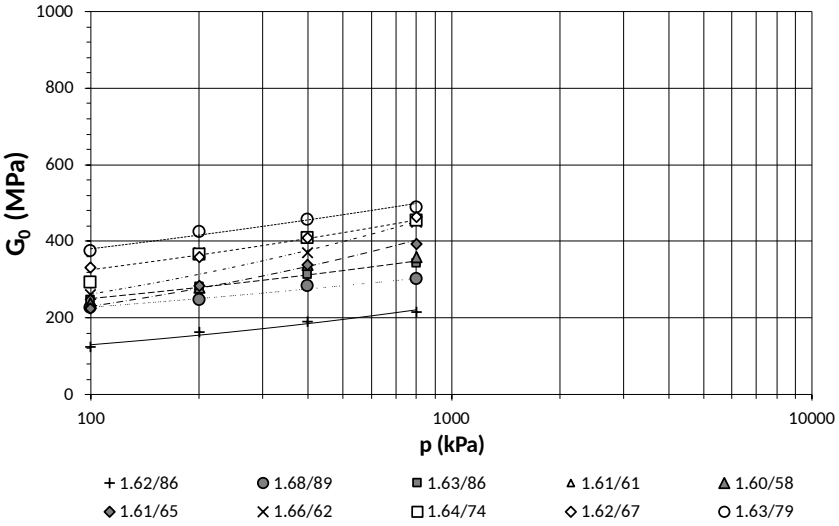

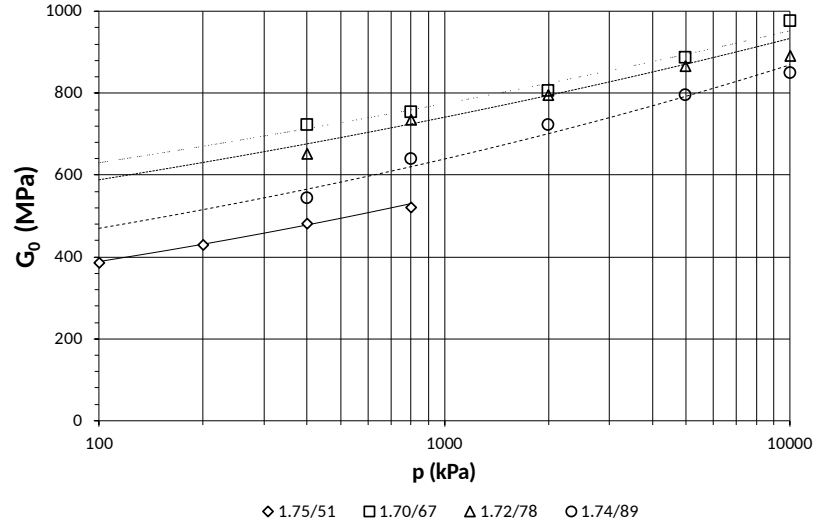

565 Figure 5. Small strain shear modulus as function of the confinement pressure in MX-80 bentonite. The
566 numbers in legend mean dry density (Mg/m^3) / degree of saturation (%).

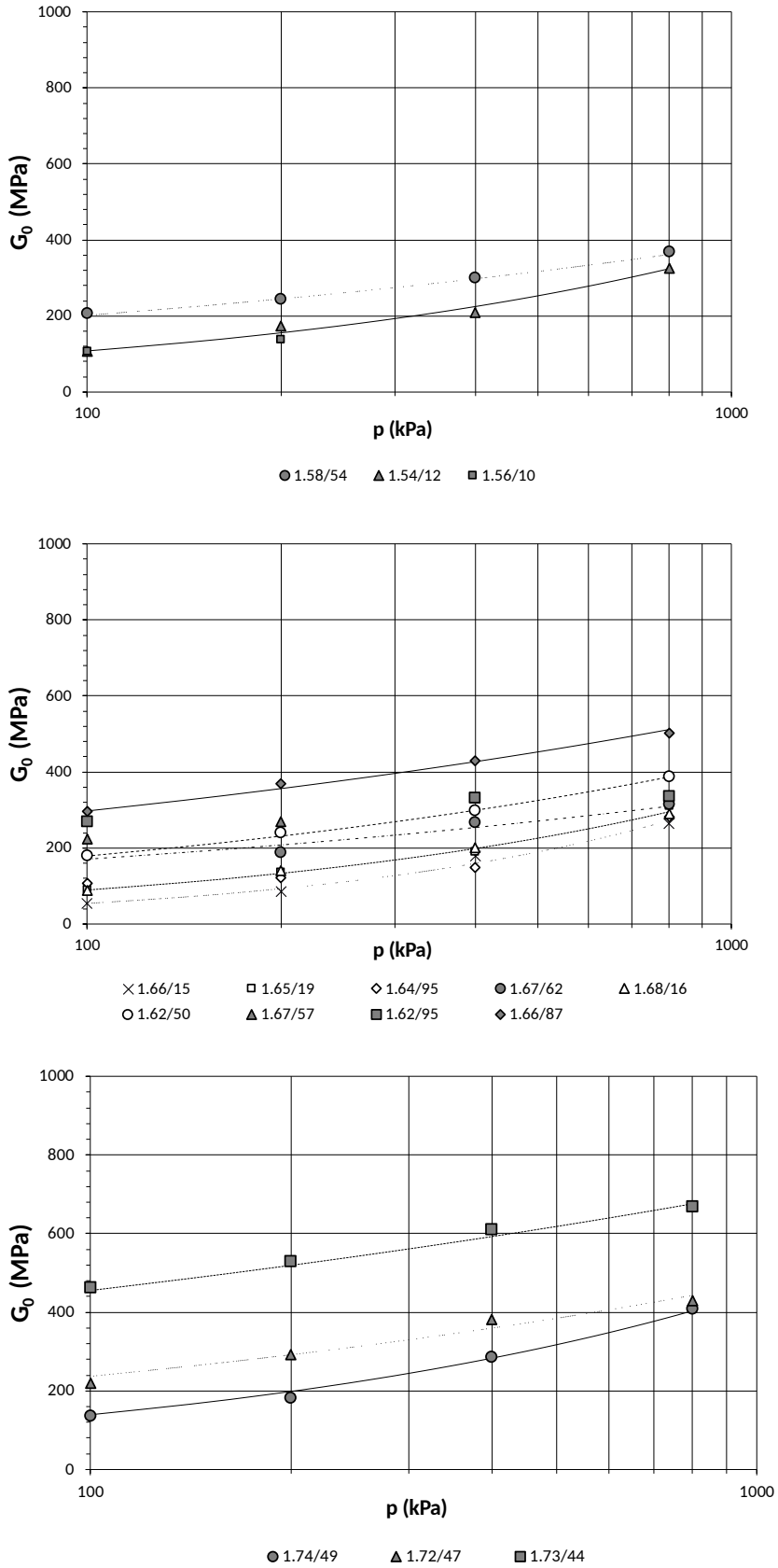

Figure 6. Small strain shear modulus as function of the confinement pressure in FEBEX bentonite. The numbers in legend mean dry density (Mg/m^3) / degree of saturation (%).

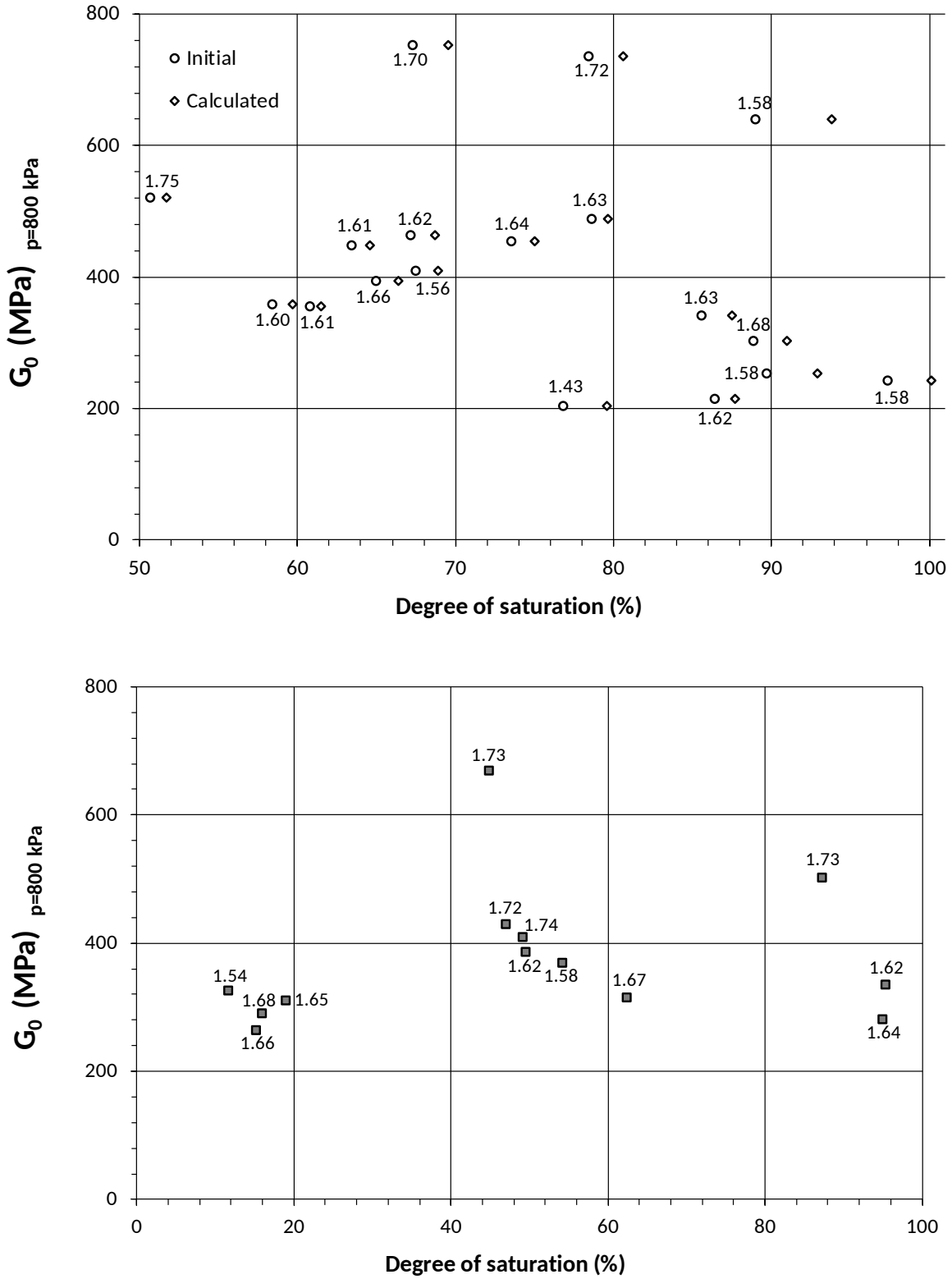

569 Figure 7. Small strain shear modulus as function of the degree of saturation for different dry densities
570 (Mg/m^3) when the confinement pressure is 800 kPa. MX-80 on top including the initial degree of
571 saturation and the degree of saturation calculated taking into account the confinement effects. For
572 FEBEX bentonite, at the bottom, only the initial degree of saturation has been considered.

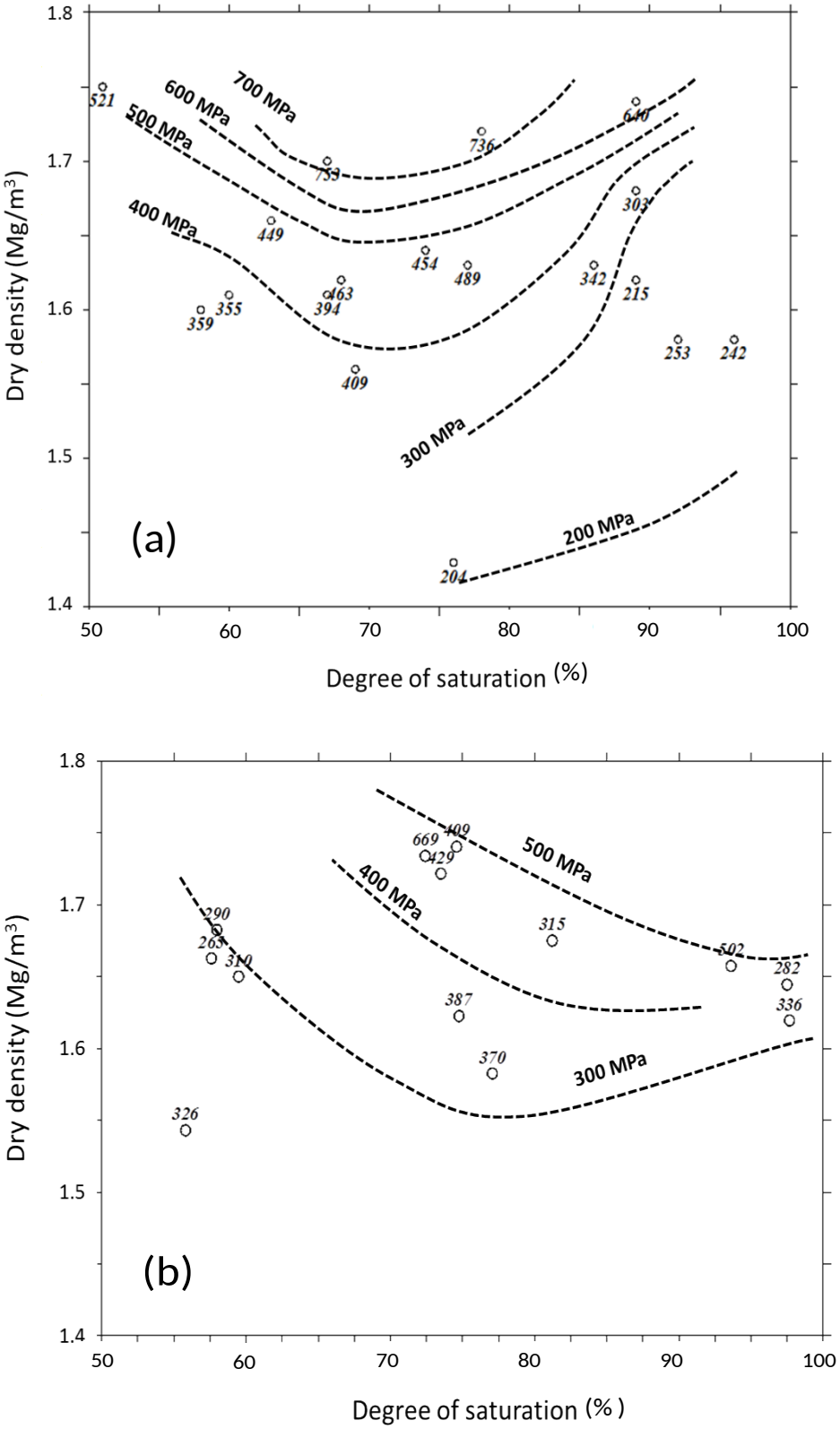

573 Figure 8. Contour plot of the small shear modulus (MPa) when the confinement pressure is 800 kPa as
574 function of initial dry density and degree of saturation. MX-80 (a) and FEBEX (b).

575

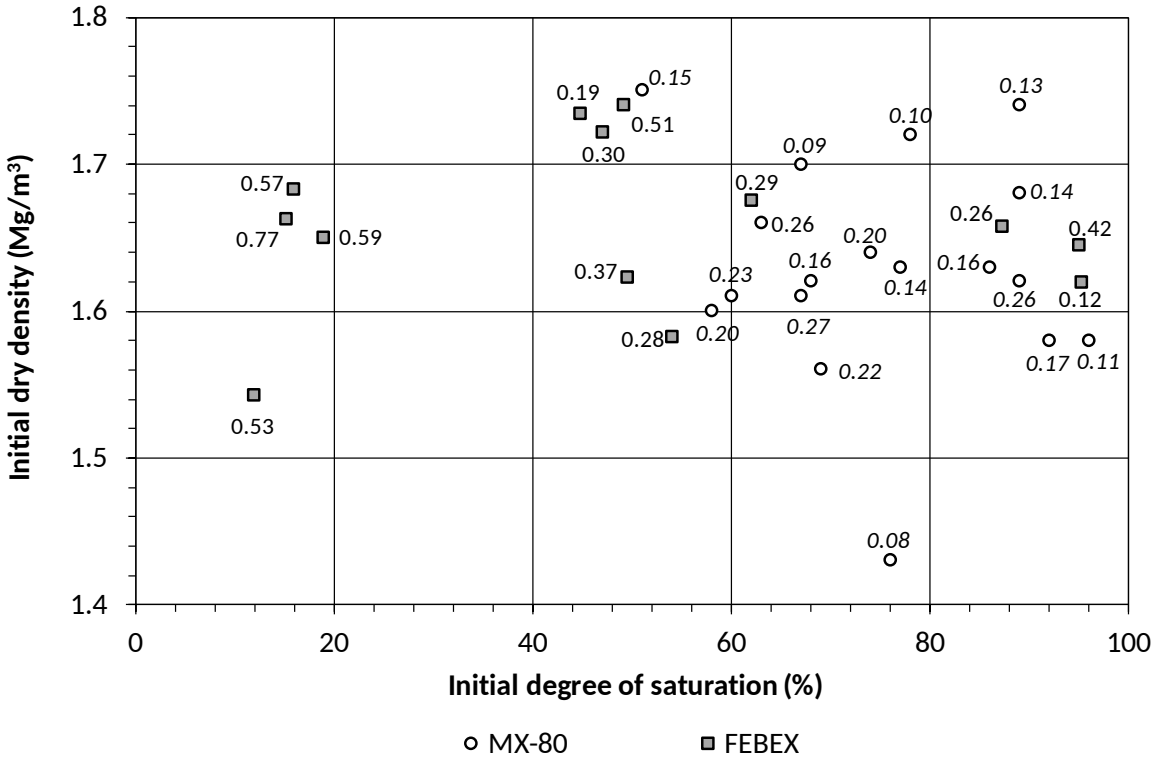

576

577 Figure 9. Value of n (equation (7)) in MX-80 and FEBEX bentonite.

578

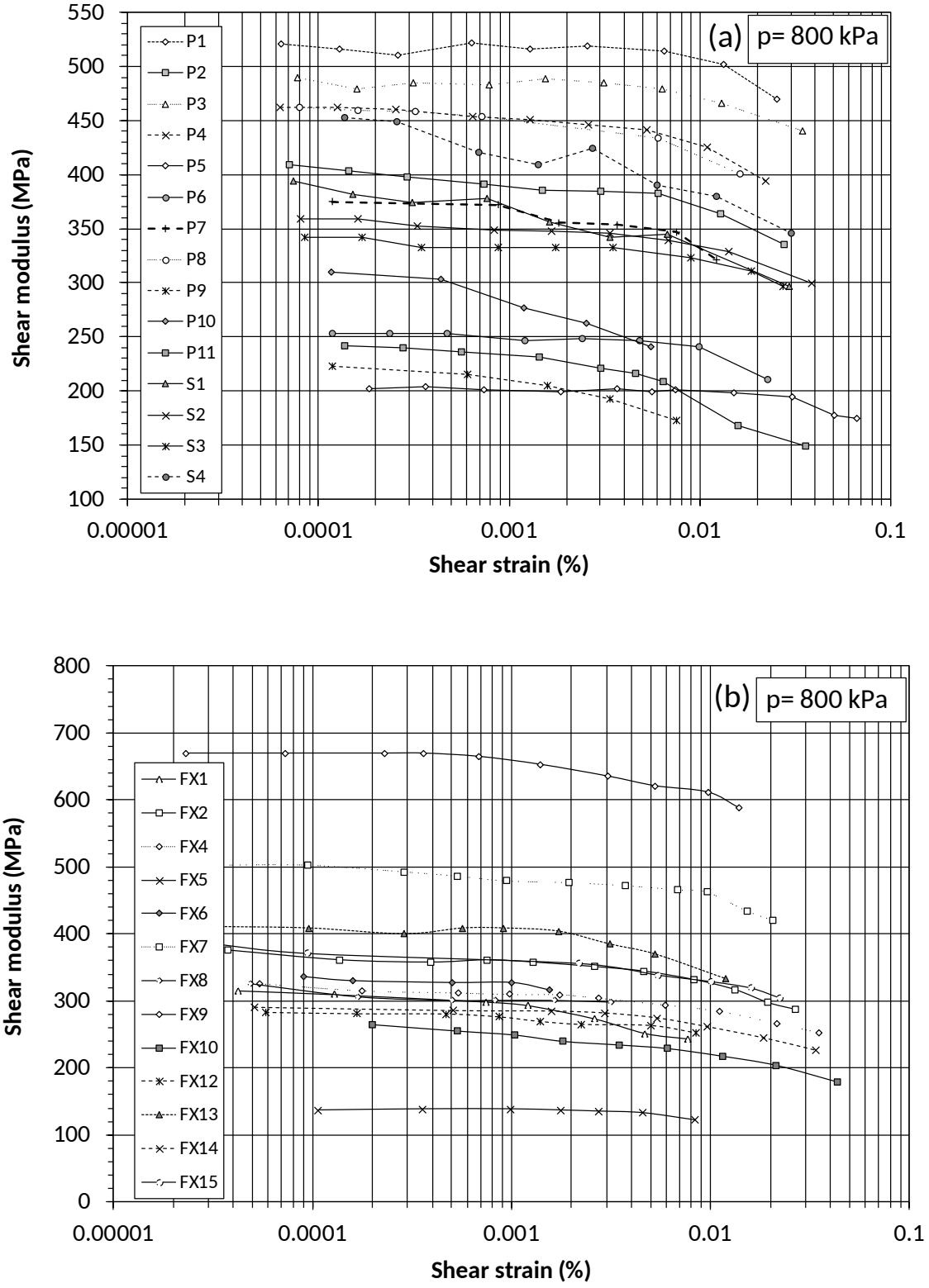

579 Figure 10. Shear modulus as function of the shear strains when the confinement pressure is 800 kPa.
580 MX-80 (a) and FEBEX (b).

581

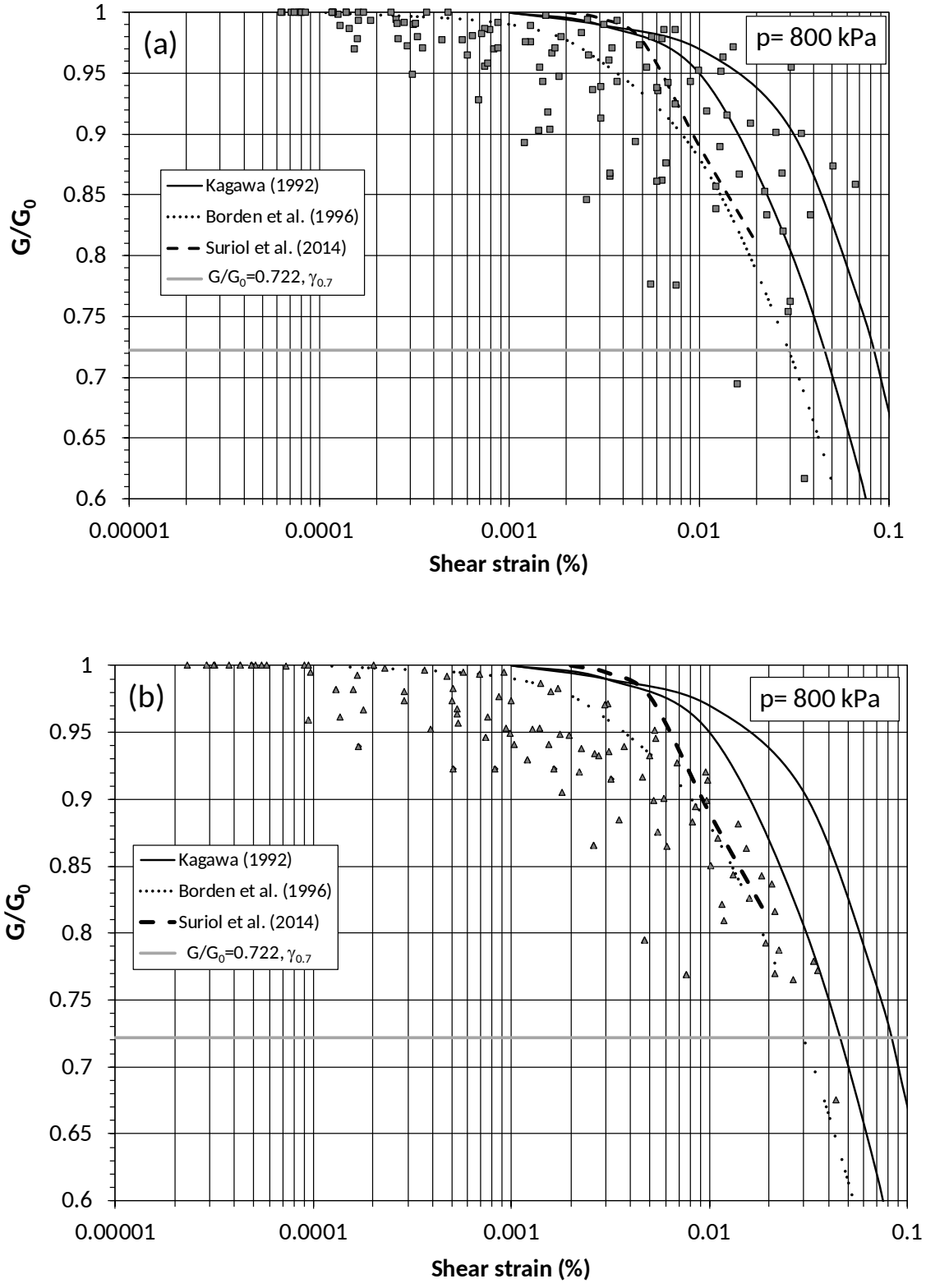

582 Figure 11. G/G_0 as function of the shear strains when the confinement pressure is 800 kPa. MX-80 (a)
583 and FEBEX (b). The results are compared with results from other authors. Kagawa (1992)[40], Suriol
584 (2014)[17] and Borden et al., 1996[42] mean the results obtained in their works.

585

586

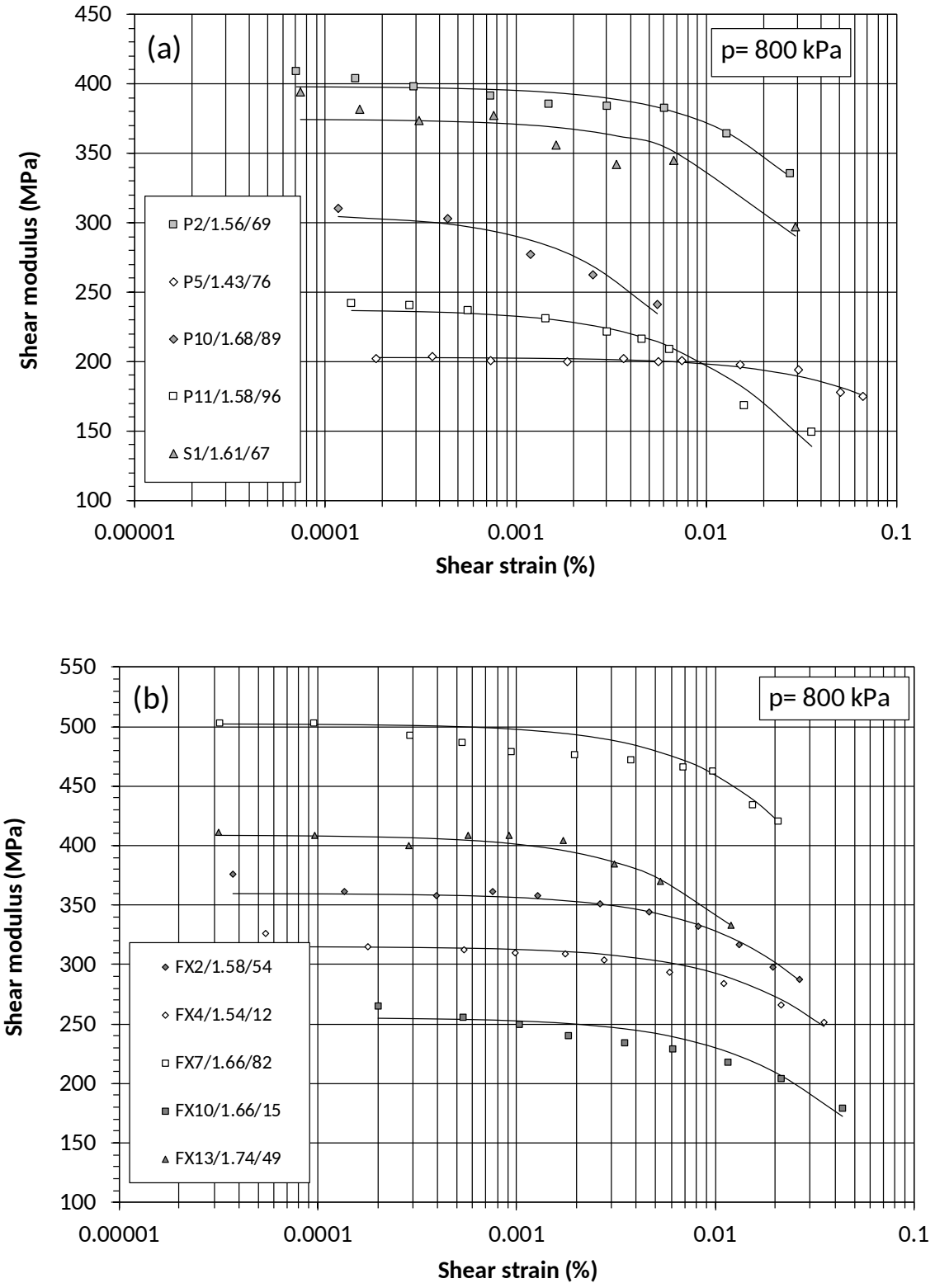

587 Figure 12. Shear modulus when the confinement pressure is 800 kPa. MX-80 (a) and FEBEX (b). The
588 numbers with the sample references are the dry density (Mg/m^3) and the degree of saturation.

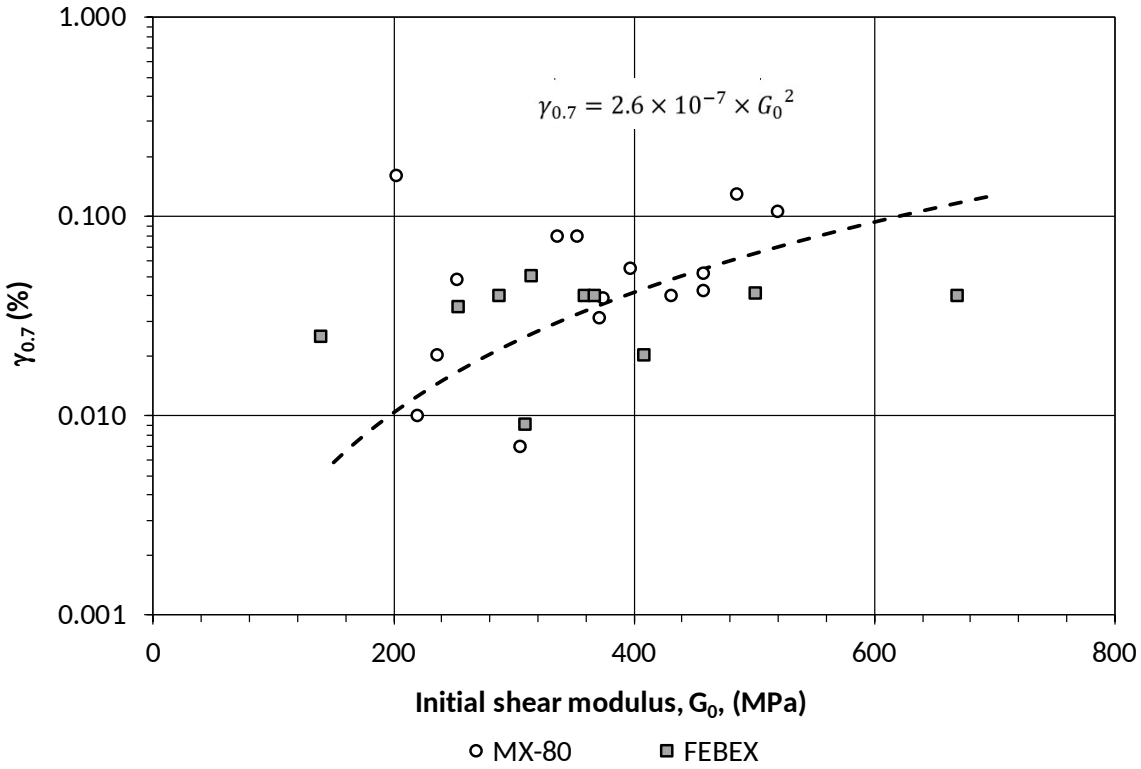

589

590 Figure 13. Value of $\gamma_{0.7}$ in MX-80 and FEBEX bentonite.

591

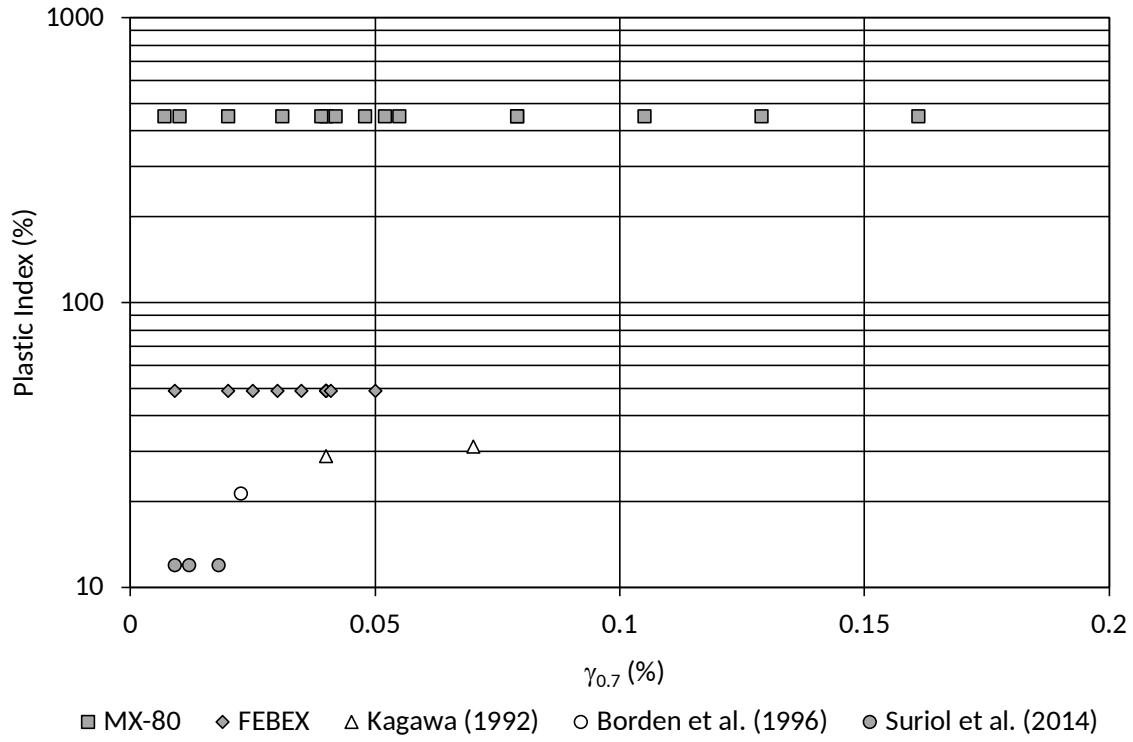

592

593 Figure 14. Plastic index vs $\gamma_{0.7}$ (%). The values of $\gamma_{0.7}$ in Kagawa (1992)[40] and Borden et al. (1996)[42]
594 were calculated from the figures and the plastic index from the tables (it had scatter and only the average
595 is showed). The values from Suriol et al. (2014)[17] corresponds to a relation G/G_0=0.8.
596

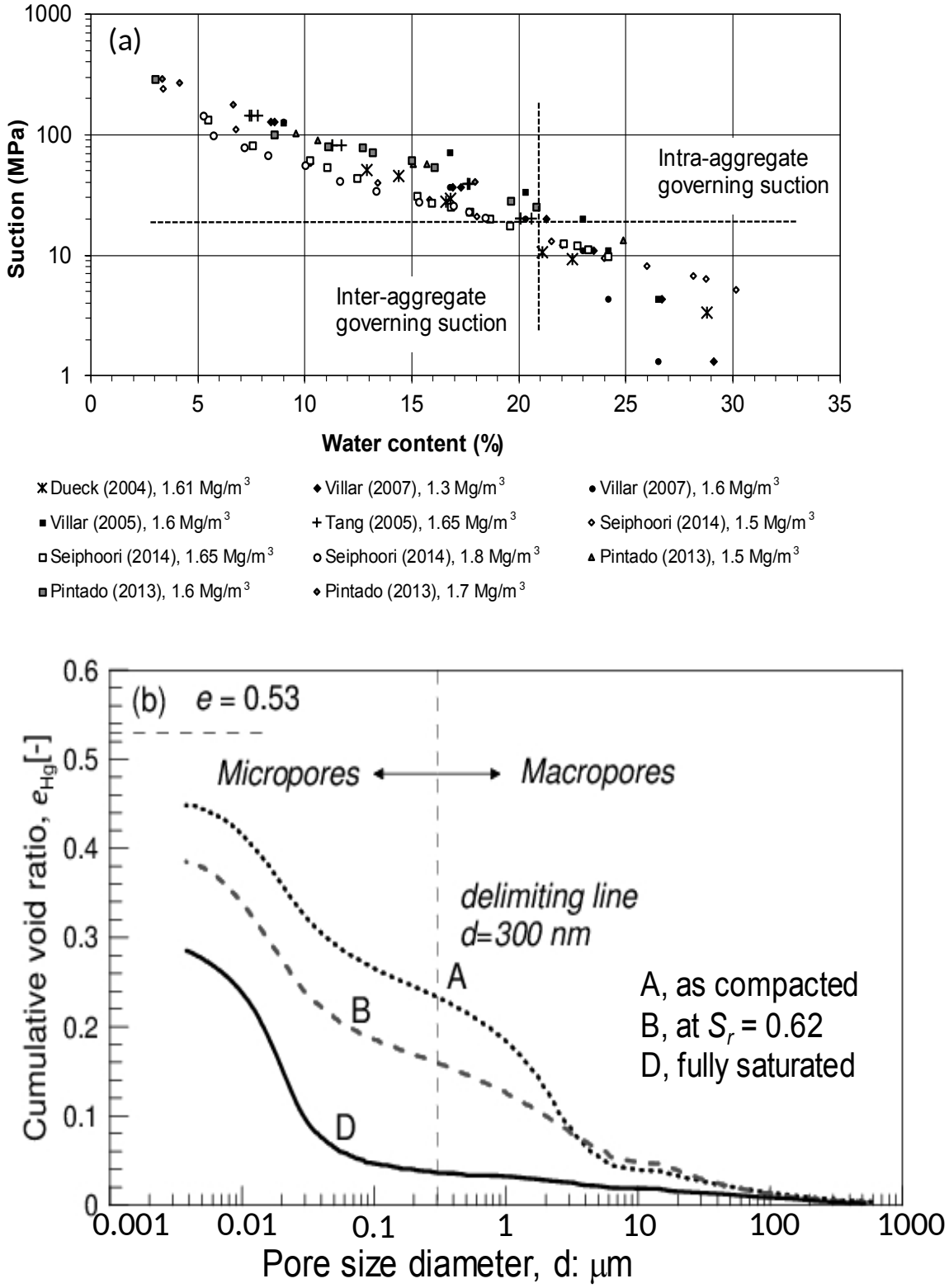

597 Figure 15. Retention curves for compacted MX-80 bentonite obtained under constant-volume conditions
598 (results from Pintado et al.[49]) (a). Relationship between pore diameter and intruded pore volume (b)
599 compacted at a dry density of 1.80 Mg/m^3 (e=0.53) with different degrees of saturation (as compacted,
600 S_r=62% and full saturated[33]).

601
602

603

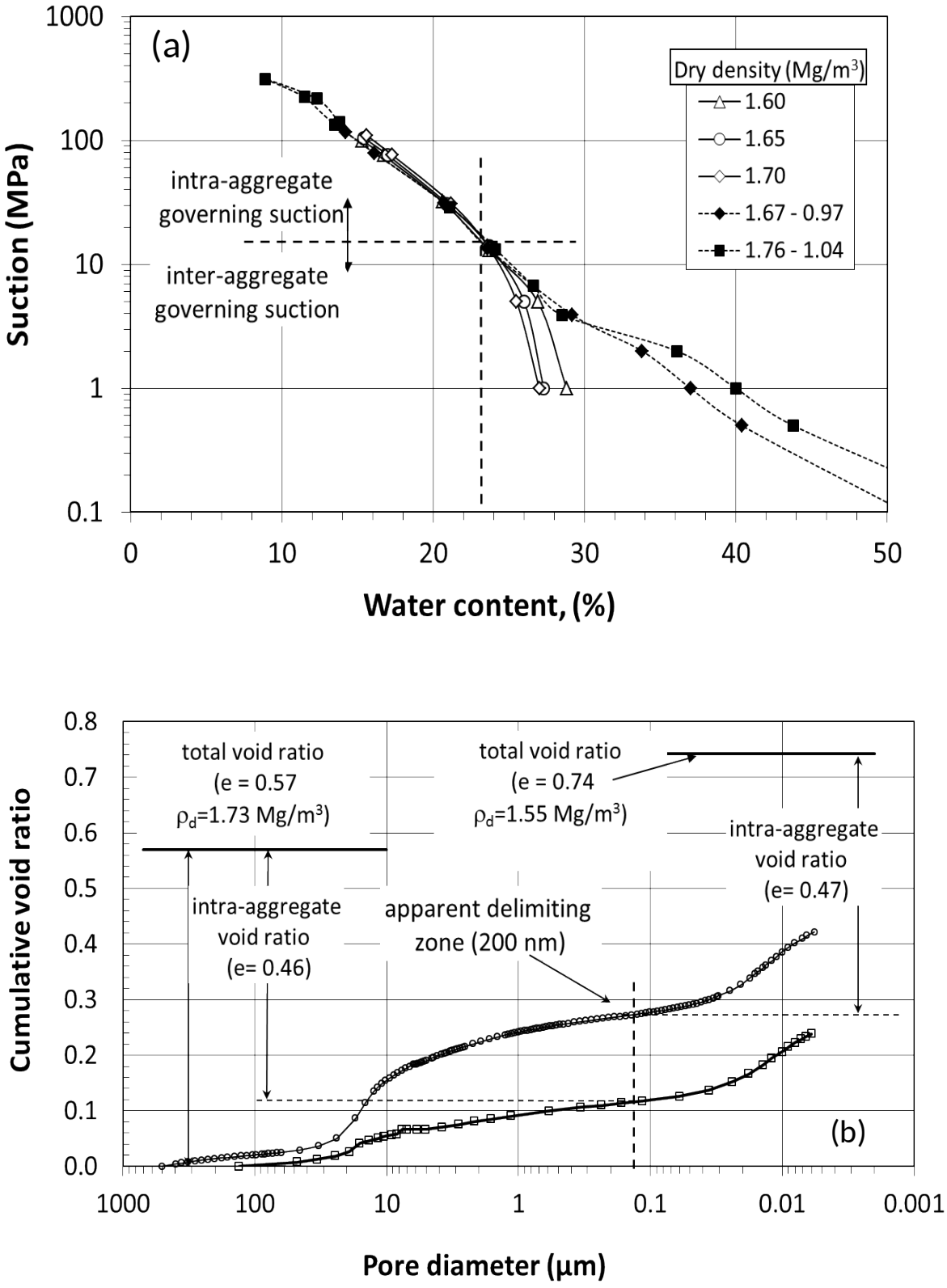

604 Figure 16. Retention curves for compacted FEBEX bentonite obtained under free swelling and constant-
605 volume conditions (a). Relationship between pore diameter and intruded pore volume for two samples
606 compacted at different dry densities in FEBEX bentonite (b)[47].

607

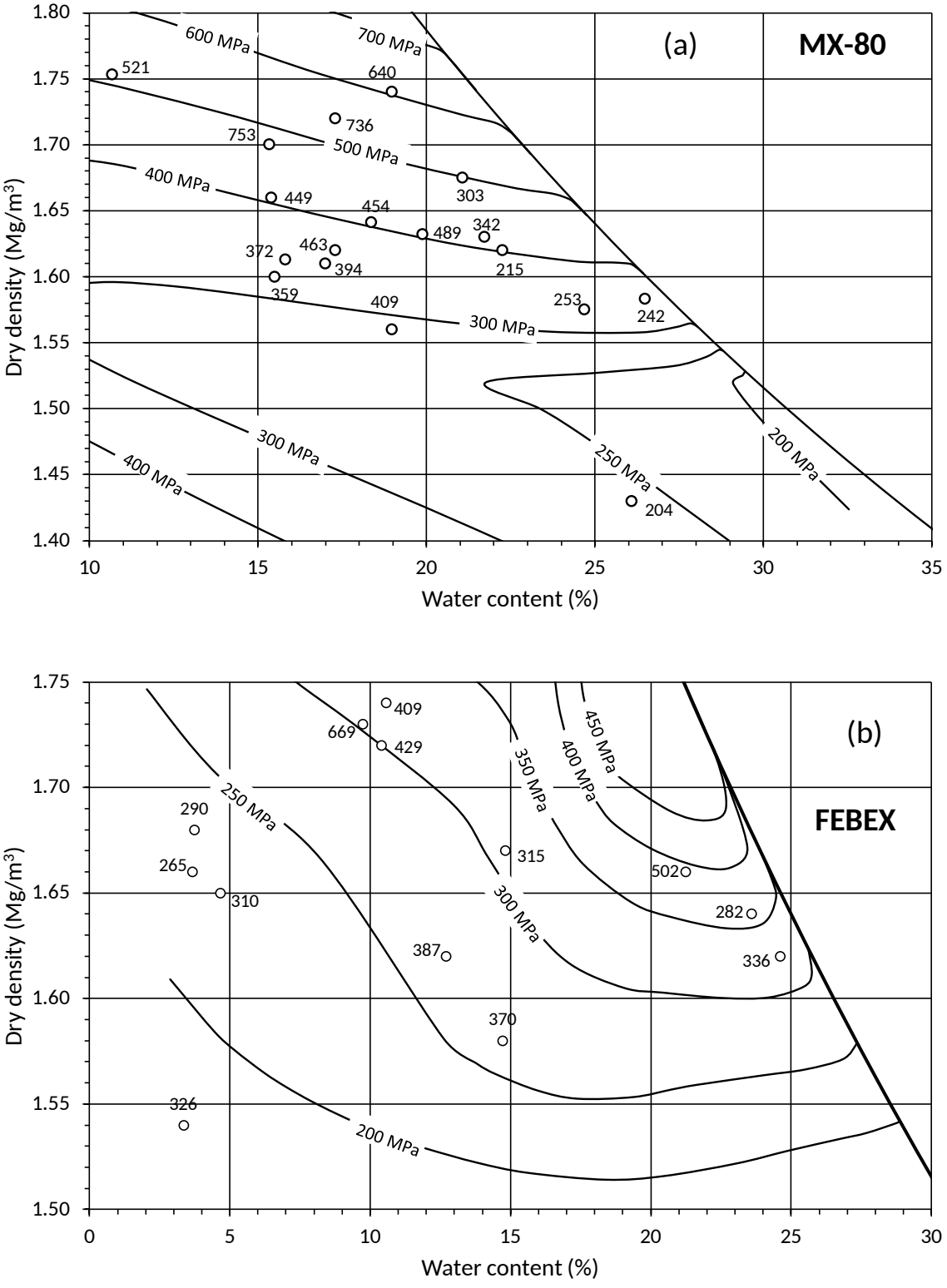

608 Figure 17. Shear modulus measured (points) and calculated (isolines) for a confinement pressure of
609 800 kPa in MX-80 (a) and FEBEX bentonite (b). The difference has been quantified following the
610 equation Error= $\sqrt{\frac{\sum_{i=1}^{n}(G_{0\,calculated,i} - G_{0\,measured,i})^2}{n}}$, where n is the number of tests. The value calculated for
611 MX-80 was 159 and for FEBEX bentonite 121.

612

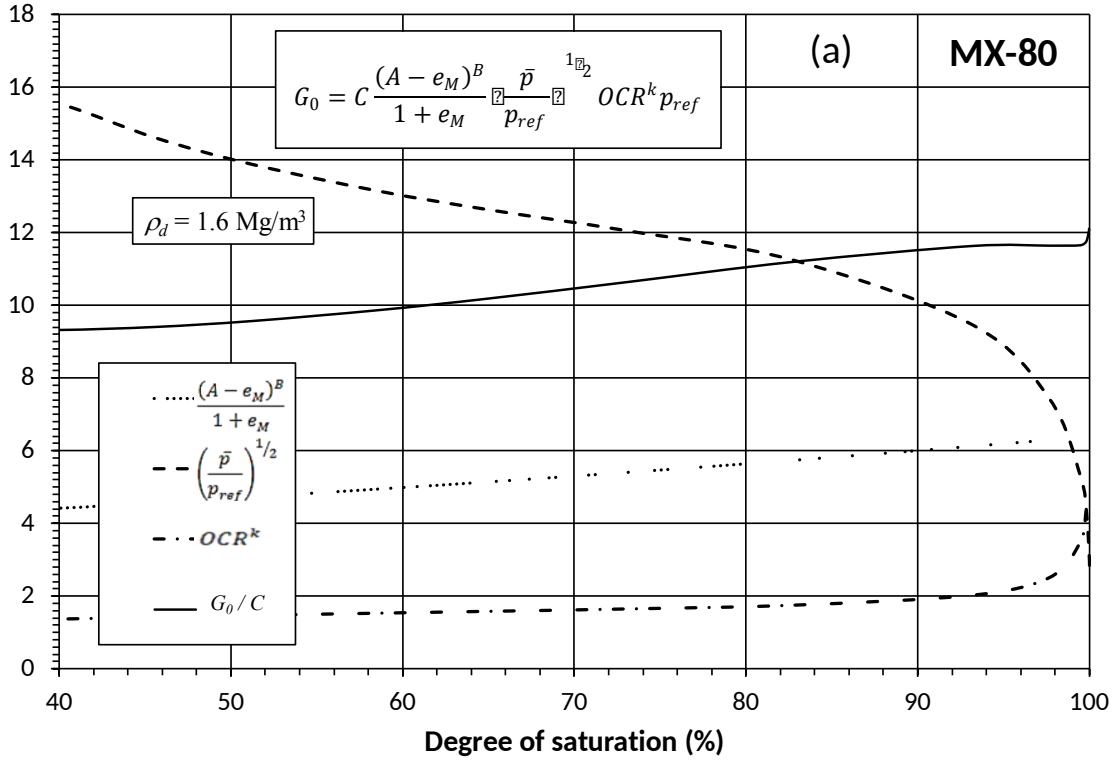

613

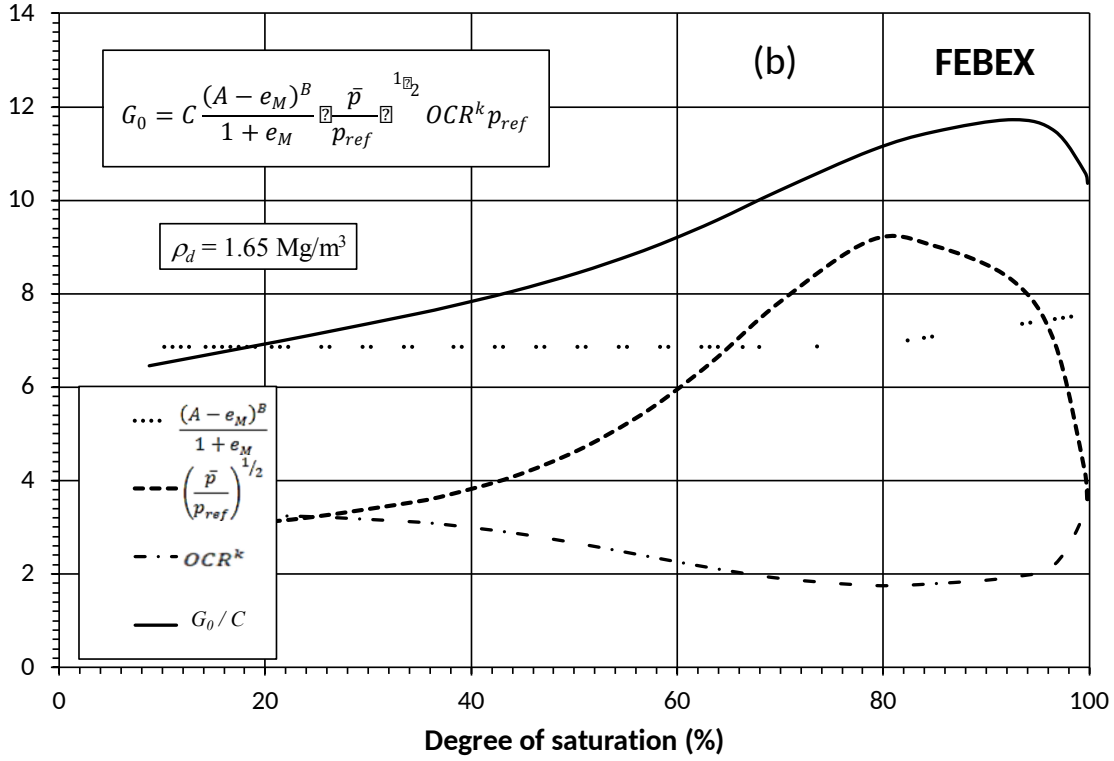

614

615 Figure 18. Variation with saturation degree of the effects on shear modulus of void ratio, constitutive
616 confining stress and overconsolidation ratio for a dry density of 1.65 Mg/m³. Results in MX-80 (a) and
617 FEBEX (b).

618

619 Table 1. Shear modulus and parameters of the models as function of the confinement pressure *p* (MPa)
620 in MX-80 bentonite.

Sample	Initial water content (%)	Initial dry density (Mg/m^3)	Initial degree of Saturation (%)	Small-strain shear modulus (G_0) in MPa						
				p=0.1	p=0.2	p=0.4	p=0.8	p=2	p=5	p=10
P1	10.7	1.75	51	386	430	481	521	-	-	-
P2	19.0	1.56	69	262	313	373	409	-	-	-
P3	19.9	1.63	77	375	424	456	489	-	-	-
P4	17.3	1.62	68	332	358	410	463	-	-	-
P5	26.1	1.43	76	169	188	193	204	-	-	-
P6	24.7	1.58	92	180	208	236	253	-	-	-
P7	15.8	1.61	60	235	275	341	355	-	-	-
P8	18.4	1.64	74	294	365	409	454	-	-	-
P9	22.3	1.62	89	124	163	190	215	-	-	-
P10	21.1	1.68	89	228	247	284	303	-	-	-
P11	26.5	1.58	96	193	221	237	242	-	-	-
S1	17.0	1.61	67	224	284	339	394	-	-	-
S2	15.5	1.60	58	239	279	338	359	-	-	-
S3	21.7	1.63	86	247	281	313	342	-	-	-
S4	15.4	1.66	63	260	370	370	449	-	-	-
HP1	15.3	1.70	67	-	-	723	753	805	888	977
HP2	17.3	1.72	78	-	-	651	736	795	866	892
HP3	19.0	1.74	89	-	-	545	640	723	795	850

621
622
623

624 Table 2. Shear modulus and parameters of the models as function of the confinement pressure *p* (MPa)
625 in FEBEX bentonite.

Sample	Initial water content (%)	Initial dry density (Mg/m^3)	Initial degree of saturation (%)	Small-strain shear modulus (G_0) in MPa			
				p=0.1	p=0.2	p=0.4	p=0.8
FX1	14.8	1.67	62		189	268	315
FX2	14.7	1.58	54	207	245	300	370
FX3	13.6	1.67	57	223	270	-	-
FX4	3.4	1.54	12	106	174	208	326
FX5	2.8	1.56	10	106	138	-	-
FX6	24.6	1.62	95	270	-	331	336
FX7	21.3	1.66	87	296	370	429	502
FX8	4.7	1.65	19	90	137	190	310
FX9	9.7	1.73	45	462	529	611	669
FX10	3.7	1.66	15	55	85	178	265
FX11	10.4	1.72	47	219	293	381	429
FX12	23.6	1.64	95	108	121	148.6	282
FX13	10.6	1.74	49	137	181	285	409
FX14	3.7	1.68	16	89	141	199.8	290
FX15	12.7	1.62	50	180	240	299	387

626

627

628 Table 3. Parameters of the model for G_0 calculation.

Soil	P_{ref} *(MPa)*	*A* *Suriol et al.*[17]	*B* *Suriol et al.*[17]	*C*	*k*	*k* *Hardin and Black*[20]
MX-80	0.1	2.97	2	32.3	0.565	0.5
FEBEX	0.1	2.97	2	32.3	0.452	0.36

629